



UNIVERSITY OF VERONA

*DEPARTMENT OF DIAGNOSTICS AND PUBLIC  
HEALTH*

*PHD SCHOOL OF HEALTH AND LIFE SCIENCES*

*PHD IN INFLAMMATION, IMMUNITY AND CANCER*

---

CYCLE: XXXI

Identifying mechanisms of resistance to MEK  
inhibition in pancreatic ductal adenocarcinoma

---

S.S.D. (Disciplinary Sector): MED/08

Coordinator: Prof. Gabriela CONSTANTIN

Signature \_\_\_\_\_

Tutor: Prof. Aldo SCARPA

Signature \_\_\_\_\_

PhD candidate: Dr. TEMGUE TANE Gael Dorien

Signature \_\_\_\_\_

Identifying the mechanisms of resistance to MEK inhibition in pancreatic  
ductal adenocarcinoma – TEMGUE TANE Gael Dorien

PhD thesis  
Verona, 22<sup>nd</sup> May 2019  
ISBN

I, TEMGUE TANE Gael Dorien, confirm that the work presented in this thesis is my own. Where information has been derived from other sources, I confirm that it has been indicated in this thesis.

I give the authorization to consult and to copy parts of this thesis for personal use only. Any other use is limited by the laws of copyright, especially concerning the obligation to refer to the source whenever and wherever results from this thesis are cited.

## Sommario

L'adenocarcinoma duttale pancreatico (PDAC) è una malattia letale senza una terapia sistemica efficace disponibile. Il PDAC è un tumore "guidato da KRAS" poiché le mutazioni attivanti della GTPasi sono quasi universali e si sono rivelate necessarie per l'avvio e il mantenimento del PDAC in modelli murini geneticamente modificati. Purtroppo nessun inibitore diretto del KRAS ha raggiunto la clinica fino ad oggi e la maggior parte degli sforzi si sono quindi concentrati sul targeting dei nodi essenziali a valle della segnalazione KRAS, inclusa la cascata della chinasi MAP. Si prevede che la monoterapia con inibitori della chinasi MAP sia inefficace a causa dell'attivazione di complessi meccanismi del circuito di retroazione che portano alla resistenza al bypass. Qui, abbiamo usato diversi modelli di PDAC per identificare i determinanti molecolari della resistenza adattativa all'inibizione della MAP chinasi utilizzando un inibitore allesterico MEK1 / 2 (trametinib, MEKi). Abbiamo dimostrato che le linee cellulari PDAC del sottotipo squamoso / basale sono più resistenti a MEKi rispetto alle cellule rappresentative del progenitore pancreatico / sottotipo classico. Indipendentemente dal sottotipo, il nostro approccio RNAseq e fosfo-proteomico ha identificato attivazione di FGFR3 come meccanismo utilizzato dalle cellule PDAC per superare il blocco MEK1 / 2 e mantenere l'output di segnalazione oncogenica. L'upregolazione trascrizionale di FGFR3 indotta da MEKi era anche evidente negli isograft di PDAC dei topi trattati continuamente con MEKi. Abbiamo inoltre eseguito analisi in silico, attraverso il database "Connettivity MAP" e test in vitro per dimostrare che l'inibizione di FGFR sensibilizza le cellule PDAC all'inibizione di MEK. Presi insieme, i nostri dati suggeriscono fortemente l'inibizione combinata di MEK e FGFR3 come potenziale trattamento per PDAC indipendentemente dal sottotipo.

## ABSTRACT

Pancreatic ductal adenocarcinoma (PDAC) is a lethal disease for which no effective systemic therapy is currently available. PDAC is a “KRAS-driven” cancer as activating mutations of the GTPase are almost universal and proved necessary for the initiation and maintenance of PDAC in genetically-engineered mouse models of the disease. Despite representing an attractive pharmacological target, no direct KRAS inhibitor reached the clinic to date and most efforts have therefore focused on targeting essential nodes downstream of KRAS signalling, including the MAP kinase cascade. Based on previous reports, monotherapy with MAP Kinase inhibitors are predicted to be ineffective due to the activation of complex feedback loop mechanisms that lead to bypass resistance. Here, we used different models of PDAC to identify molecular determinants of adaptive resistance to inhibition of MAP Kinase using an allosteric MEK1/2 inhibitor (trametinib, MEKi). We showed that PDAC cells lines that align with the squamous/basal-like subtype are more resistant to MEKi as compared to cells representative of the pancreatic progenitor/classical subtype. Regardless of the subtype, our integrative RNAseq and phospho-proteomic approach identified activation of FGFR3 as mechanisms used by PDAC cells to overcome MEK1/2 blockade and maintain the index oncogenic signalling output. MEKi-induced transcriptional upregulation of *FGFR3* was also evident in mouse PDAC isografts treated continuously with MEKi. We further performed *in silico* analysis, through the Connectivity Map database, and *in vitro* drug-testing to demonstrate that FGFR inhibition sensitize PDAC cells to MEK inhibition. Taken together, our data strongly suggest combined inhibition of MEK and FGFR3 as potential treatment for PDAC regardless of the subtype.

## Acknowledgements

I am blessed to have exceptional parents, TANE Pierre and TSAPI Prisca, who spared no efforts to give me a wonderful education. Thanks to Geraldin TANEKEU, my little brother, and my Grandma NODEM Jeannette that has never ceased to pray for despite the distance.

I give thanks to the Almighty for having given me an exceptional spouse like Jeanne Gaetane TEMGUE whose emotional and spiritual support were invaluable during this long journey. " Merci Mama leki de moi seul".

Thanks to fathers TSONA Francis, NZOYEM Gabriel, YEMENE Augustin, NANGUEU Bruno, my moms TSONA Henriette, NZOYEM Marie, NANGUEU Marinette, CHIASSA Marie-Bonheur for all their support and their parental love. Thanks to my brothers and sisters Sandra, Tatiana, Darling, Josias, Christelle, Achille, Fatima, Raissa, Christabel, Belmond, for all their prayers and encouragements.

Thanks, to my family-in-law, Kevine, Bruno, Librich and Vanessa CHIASSA.

Merci plein d'affection à Merveille DE TCHADJET, ma bien aimée fille, "lacoucou de papi".

Thanks a lot to Alain TENOH, more than a friend, a brother.

I give thanks to the Lord for the presence of these wonderful people that have been of great spiritual and psychological support for me: TCHAPDA Elie Bertrand's family, DJASING Patrick's family, NANA Amavie, Olive DE TCHADJET, Mathilde MONTHE MOUALE, Diane KANKEU, Pamela MOMO, Blanche, Mathurin MFEE, and all brothers and sisters in the Lord.

Blessings you are brothers and sisters, Michael NGOUADJEU, Gaelle AZEBAZE, Sorelle NZOULO and Alex MABOU TAGNE.

I'm grateful to Prof. Aldo SCARPA for the opportunity he gave me in his laboratory to accede to doctoral studies in cancer research.

I will miss words to say thank to Dr. Vincenzo CORBO for his teachings, his follow-up and his unparalleled closeness.

An infinite “Grazie mille con tanti baci” to Claudia FIORINI for her very maternal and affectionate follow-up, for her encouragements and her willingness to help me achieve academic goals and even beyond.

I will not forget to say “Merci infiniment” to Anais Del CURATOLO for her kindness, her sympathy and her very friendly advices.

I'm grateful to all the other elders of the laboratory, namely Francesca Lупpo, Sabrina D'AGOSTO, Michele SIMBOLO, Caterina VICENTINI, Andrea MAFFICINI, Stefano BARBI, Davide ANTONELLO, and Giorgio MALPELLI.

Many thanks to my lab-mates and colleagues, Dea FILIPPINI, Tasos GKOUNTAKOS, Elena FIORINI, Lisa VEGHINI and Silvia ANDREANI.

All my gratitude to Giona TURRI, Maria SCARDONI, as well as all the technical staff of the Laboratory of Pathological anatomy of the University of Verona and of Arcnet Research Center.

Gratitude to all the pharmacists and coordinators of the URCA-DSCHANG project.

Better *is* the end of a thing than the beginning thereof: *and* the patient in  
spirit *is* better than the proud. Eccl.7:8

**To the Lord my God, to my wife Jeanne Gaetane TEMGUE and  
my beloved family.**

# TABLE OF CONTENTS

|   |    |
|---|----|
| Sommario.....                                 | 4  |
| Abstract .....                                | 5  |
| List of Figures .....                         | 11 |
| List of Tables .....                          | 12 |
| List of abbreviations.....                    | 13 |
| 1 Introduction .....                          | 14 |
| 1.1 Pancreatic cancer: the state of art ..... | 14 |
| 1.2 Pathophysiology.....                      | 15 |
| 1.3 Molecular biology.....                    | 16 |
| 1.4 The rational of this thesis.....          | 14 |
| 2 Materials and Methods.....                  | 26 |
| 2.1 Materials.....                            | 26 |
| 2.2 Methods .....                             | 28 |
| 3 Results & Discussion.....                   | 38 |
| 4 Conclusions .....                           | 60 |
| 5 Bibliography.....                           | 63 |
| 6 Appendix.....                               | 67 |

## List of figures

**Figure a.** Model of three distinct morphological pathways to invasive pancreatic carcinoma.

**Figure b.** Landscape of Genomic Alterations in Pancreatic Ductal Adenocarcinoma.

**Figure c.** The main classifications of PDAC subtypes and impact of the purity on the molecular analysis.

**Figure d.** Kaplan–Meier analysis of patient survival stratified by class.

**Figure e.** KRAS regulation and effector signalling.

**Figure f.** Anti-Ras drug discovery.

**Figure 1.** Subtyping of PDAC cell lines.

**Figure 2.** MEK inhibitor efficacy in PDAC cell lines.

**Figure 3.** MEKi induce kinome reprogramming in PDAC cell lines.

**Figure 4.** Potential mechanisms of increased FGFR3 expression in PDAC following MEK inhibition.

**Figure 5.** Connectivity MAP analyses nominated candidates for combinatorial treatment.

**Figure S1.** MEKi induces kinome reprogramming in vivo (Appendix).

**Figure S2.** Phospho-RTK analysis of PDAC cell lines treated with MEKi (Appendix).

## List of tables

**Table 1.** PDAC sequencing studies.

**Table 2:** List of probes used during this project.

**Table 3.** List of antibodies used for western blot and immunohistochemistry.

**Table 4.** Mutations of PDAC “driver” genes in the 6 cell lines used in the study.

**Table 5.** EC50 concentration of 72 hours MEKi treatment of PDAC cell lines

**Supplementary Table 1.** Tyrosine Kinase genes deregulated following MEKi in human PDAC (related to Figure 3b, Appendix)

**Supplementary Table 2.** List of 300 deregulated genes used for CMAP analysis (related to Figure 5, Appendix)

## List of abbreviations

ADEX: aberrantly differentiated endocrine exocrine  
AKT: *protein* kinase B  
ATP: Adenosine triphosphate  
BRCA: Breast Related Cancer Antigens  
CDKN2A: Cyclin Dependent Kinase Inhibitor 2A  
DAPI: 4',6'-diamidino-2-phenylindole  
DMSO: dymethyl sulfoxide  
DNA: Deoxy-ribo-nucleic acid  
DPBS: *Dulbecco's Phosphate Buffered Saline*  
DUSP: Dual-specificity phosphatase  
EGFR: Epithelial growth factor receptor  
ERK: Mitogen-activated *protein* kinase  
FGF: fibroblast growth factor  
FGFR: fibroblast growth factor receptor  
GSVA: gene set variation analysis  
GTP: guanosine triphosphate  
IPMN: Intraductal papillary mucinous neoplasms  
KRAS: V-Ki-ras2 Kirsten rat sarcoma viral oncogene homolog  
MCN: mucinous cystic neoplasm  
MEK: Mitogen-activated *protein* kinase kinase  
mTOR: mammalian target of rapamycin  
PanIN: Pancreatic intra-epithelial neoplasia  
PDAC: Pancreatic ductal adeno-carcinoma  
QM-PDA: Quasi-mesenchymal pancreatic ductal adenocarcinoma  
RNA-Seq: Ribo nucleic acid sequencing  
RTK: receptor tyrosine kinases  
RT-PCR: real-time quantitative polymerase chain reaction  
SMAD4: Mothers against decapentaplegic homolog 4  
TCGA: The Cancer Genome Atlas  
TP53: Tumor protein 53  
WHO: World Health Organisation

# 1 Introduction

## 1.1 Pancreatic cancer: the state of art

Pancreatic Ductal Adenocarcinoma (PDAC) is the most common malignancy of the pancreas. It is actually the 4th highest cause of cancer death, and it is expected to be the second cause of cancer death by 2030 in Western countries, despite representing only 3% of new cancer diagnosis <sup>1</sup>. Although the aetiology of pancreatic cancer remains unclear, there are genetic conditions and accepted risk factors that include smoking, family history of chronic pancreatitis, advancing age, diabetes mellitus, obesity, non-O blood group associated to PDAC cancer risk development. Among the syndromes that can cause pancreatic cancer there are Peutz Jeghers syndrome, *BRCA2* gene mutation, familial pancreatitis caused by mutations in the gene *PRSS1*, and Lynch syndrome <sup>2</sup>. Although the cause of pancreatic cancer is complex and multi factorial, cigarette smoking and family history are dominant.

Unfortunately, when the tumour becomes symptomatic most patients already present locally advanced or metastatic disease and surgical resection remains the only effective therapeutic option. Recently, the combinations of fluorouracil, irinotecan, oxaliplatin, and leucovorin (FOLFIRINOX) or gemcitabine plus albumin bound paclitaxel particles (nab- paclitaxel) has shown to improve the survival of metastatic PDAC patients compared with gemcitabine <sup>3</sup>. Targeted approaches have constantly failed in the advanced PDAC setting. For these reasons, the research of an effective treatment is the most important challenge in PDAC clinical oncology<sup>4-6</sup>.

## 1.2 Pathophysiology

Pancreas has two different units, endocrine and exocrine, which have different functions: the exocrine tissue represents the 80% of the organ and is mostly composed of acinar cells which produce digestive zymogens. The endocrine tissue (Islets of Langerhans) is located in the tail region of pancreas. The most common type of pancreatic cancer is the pancreatic ductal adenocarcinoma (PDAC) and it derives from the exocrine unit. Pancreatic cancer is characterized by a step-wise progression to a malignant status from benign precursor lesions. Pancreatic intraepithelial neoplasia (PanIN), intraductal pancreatic mucinous neoplasm (IPMN) and mucinous cystic neoplasm (MCN) represent the three well known PDAC precursor lesions (**Figure a**). In particular, PanINs are the most common lesions and they can be classified from stage 1 (A-B) to stage 3. PanIN-3 is associated with cytonuclear abnormalities, but the growth is non-invasive. Among the premalignant lesions, there have been found common molecular events such as activating point mutations in codon 12 of the *KRAS* gene, and also mutations in tumour-suppressor genes: *CDKN2A*, *TP53*, *BRCA*, and *SMAD4*<sup>7 8</sup>. Another type of lesions is intraductal papillary mucinous neoplasms (IPMNs) that are mucin producing lesions, which might progress from benign adenomas to invasive carcinoma. These neoplasms extensively involve the main pancreatic ducts and/or major side branches<sup>9</sup>.

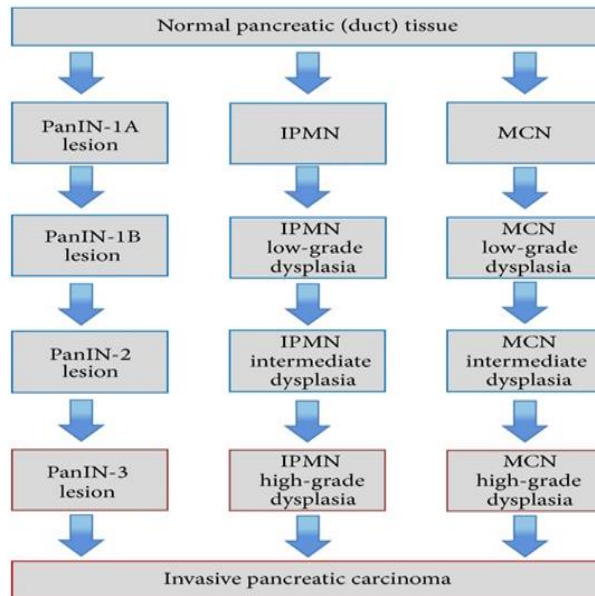


**Figure a. Model of three distinct morphological pathways to invasive pancreatic carcinoma<sup>10</sup>.**

### 1.3 Molecular Biology of PDAC

Pancreatic ductal adenocarcinoma (PDAC) constitutes more than 90% of pancreatic cancers in humans. It's a devastating and virtually unexceptionally lethal malignancy, afflicting around 213,000 individuals worldwide every year<sup>11</sup>. The most frequent genetic alterations in invasive pancreatic adenocarcinoma are aberrant activation of the *KRAS* oncogene, inactivation of tumour suppressor genes including *CDKN2A*, *TP53*, *SMAD4*, and *BRCA*, widespread chromosomal losses, gene amplifications, and telomere shortening. *KRAS* has a central role in PDAC tumorigenesis; it is involved in different cellular functions such as differentiation, proliferation and survival. Activating mutations within the *KRAS* oncogene are present in up to 90-95% of pancreatic cancers, most commonly affecting codon 12 but also 13 or 61. The activating mutations abolish the intrinsic control of the GTPase activity, resulting in constitutive

activation of intracellular signal transduction. *KRAS* mutation is not only the most frequent genetic abnormalities in pancreatic cancer but it is suspected to be the earliest changes observed in non-malignant precursor-lesions, already being present in about 30% of preinvasive PanIN-1 lesions<sup>12</sup>. Other genes, mutated in up to 20% of pancreatic cancers, include oncogenes such as *BRAF*, *MYB*, *AKT*, and *EGFR*, and tumour suppressor genes such as *MAP2K4*, *STK1*, *TGFBR2*, *ACVR1B*, *ACVR2A*, *FBXW7*, and *EP300*<sup>13</sup>. Whole-exome sequencing studies also identified additional recurrent mutations in PDAC; however, the prevalence of individual mutations drops to  $\leq 10\%$  (**Table 1, Figure b**). It's worth to note that this large number of diverse gene mutations converge on many pathways and processes, including NOTCH, Hedgehog (Hh),  $\beta$ -catenin, axon guidance, chromatin remodelling, and DNA repair pathways. This suggests that majority of these mutations may function through certain processes, which may offer key nodal points for therapeutic intervention<sup>14</sup>. Similar to other cancer types, one major class of frequently mutated genes in PDAC is involved in the regulation of the epigenome, including histone modification enzymes (24% of PDAC) and SWI/SNF-mediated chromatin remodelling complexes (14% of PDAC). Among the mutated histone modification enzymes are the histone methyltransferases *MLL*, *MLL2*, and *MLL3* and the histone demethylase *KDM6A*<sup>14</sup>. However, the biology of these chromatin regulators and how they are involved in cancer progression and/or suppression are not well understood and appear to be highly specific to the context. PDAC also exhibits gain/amplification oncogenes such as *MYC* and some protein kinases such as *ROIK3*<sup>15</sup>. *MYC* amplification worsen the prognosis. Moreover, *MYC* is critical for oncogenic Kras-driven tumour maintenance in many cancer types, and its suppression leads to rapid and sustained tumour regression in preclinical models.

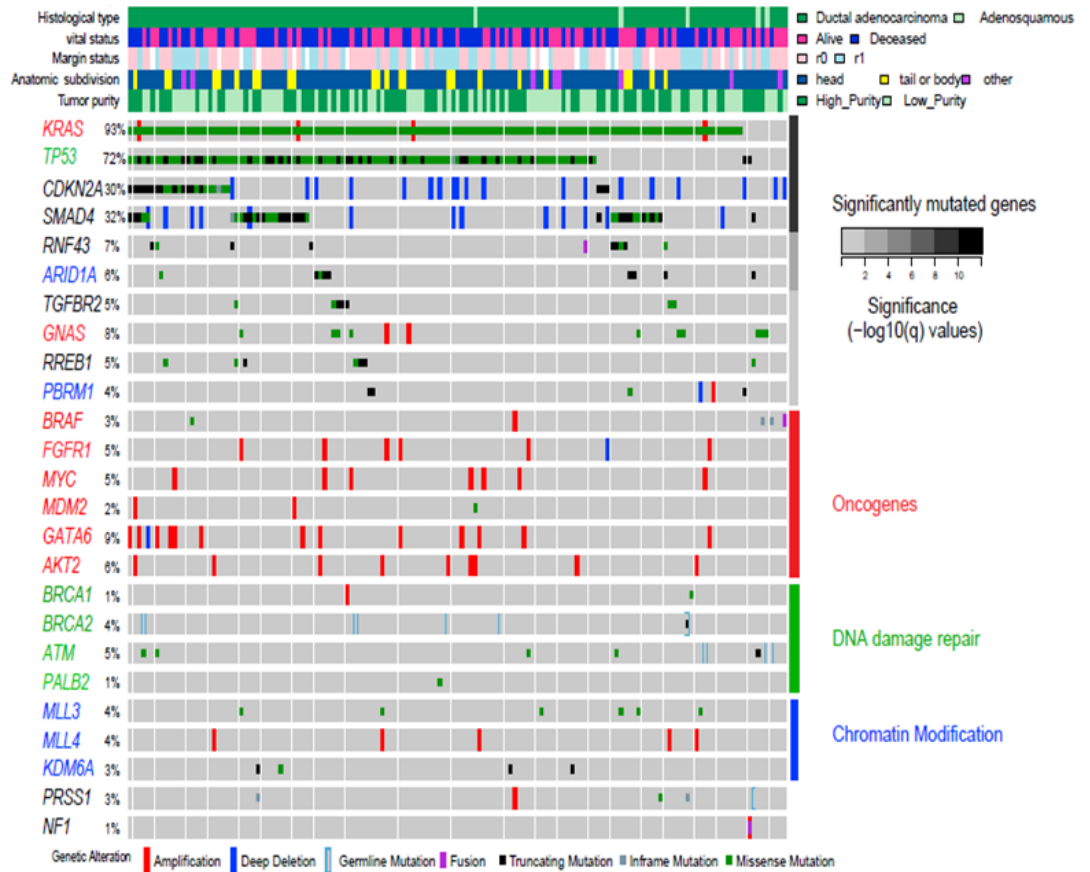


**Figure b. Landscape of Genomic Alterations in Pancreatic Ductal Adenocarcinoma<sup>16</sup>.**

**Table 1. PDAC sequencing studies.**

| Author       | Publication Year | Number of cases | Method   |
|--------------|------------------|-----------------|--|
| Jones S      | 2008             | 24              | Exome sequencing   |
| Yachida S    | 2010             | 7               | Exome sequencing   |
| Campbell PJ  | 2010             | 13              | Parallel paired-end sequencing   |
| Collisson EA | 2011             | 2 databases     | Gene expression microarray   |
| Biankin AV   | 2012             | 99              | Whole-genome sequencing;<br>Copy number variation analysis               |
| Moffitt RA   | 2015             | 206             | Gene expression microarray   |
| Waddell N    | 2015             | 100             | Whole-genome sequencing;<br>Copy number variation analysis               |
| Bailey P     | 2016             | 456             | Whole-genome sequencing;<br>Deep exome sequencing;<br>CNV analysis       |
| Raphael BJ   | 2017             | 150             | genomic, transcriptomic, and proteomic profiling, Whole exome sequencing |

Genome- and gene expression-based subtypes have been widely accepted as methods for disease stratification. The first impactful PDAC molecular subtyping study was published by Collisson et al <sup>17</sup> and identified three subtypes (classical, quasi-mesenchymal (QM-PDA) and exocrine-like) based on different gene expression profiles.

In particular, these three subgroups were characterized by high expression of adhesion-associated and epithelial genes (classical), mesenchyme-associated genes (QM-PDA), and tumour cell-derived digestive enzyme genes (Exocrine-like)<sup>17</sup>.

In 2015, Moffitt et al. identified two stromal subtypes ('normal' and 'activated') and two neoplastic cell subtypes ('classical' and 'basal-like') of PDAC. The most recent mRNA-based classification proposed by Bailey and colleagues describes four main molecular subtypes: squamous, pancreatic progenitor; immunogenic; aberrantly differentiated endocrine exocrine (ADEX)<sup>18</sup>.

Squamous tumours comprised mutated *TP53* and *KDM6A* genes, an upregulated TP63ΔN transcriptional network and hypermethylated pancreatic endodermal cell genes, while pancreatic progenitor tumours expressed genes implicated in early pancreatic development (FOXA2/3, PDX1 and MNX1). Immunogenic tumours showed upregulation of immune networks, including pathways involved in developed immune suppression. Finally, ADEX tumours were characterized by high expression of genes induced by KRAS activation, exocrine differentiation (NR5A2 and RBPJL), and endocrine differentiation (NEUROD1 and NKX2-2)<sup>18,19</sup>.

Morphologically, PDACs are characterized by a desmoplastic reaction with a dense fibrotic stroma and limited neoplastic cells content. The paucity of neoplastic cells in PDAC tissues is a confounding factor for both genomic and transcriptomic analyses. Recently, Raphael et al.<sup>16</sup> proposed the classification of samples as basal-like or classical, which was independent of purity, and based on intrinsic characteristics of neoplastic cells. They found that, among low-purity tumours, a higher estimated leukocyte fraction was associated with immunogenic samples of Bailey<sup>18</sup>. Further, the ADEX class was a subdivision of the exocrine-like class. Considering only the

high-purity samples in their cohort, the squamous samples of Bailey<sup>18</sup> showed significant overlap with the basal-like samples defined by Moffitt<sup>20</sup>, while the Bailey pancreatic progenitor and classical group from Collisson<sup>21</sup> overlapped the classical samples defined by Moffitt (Figure c).

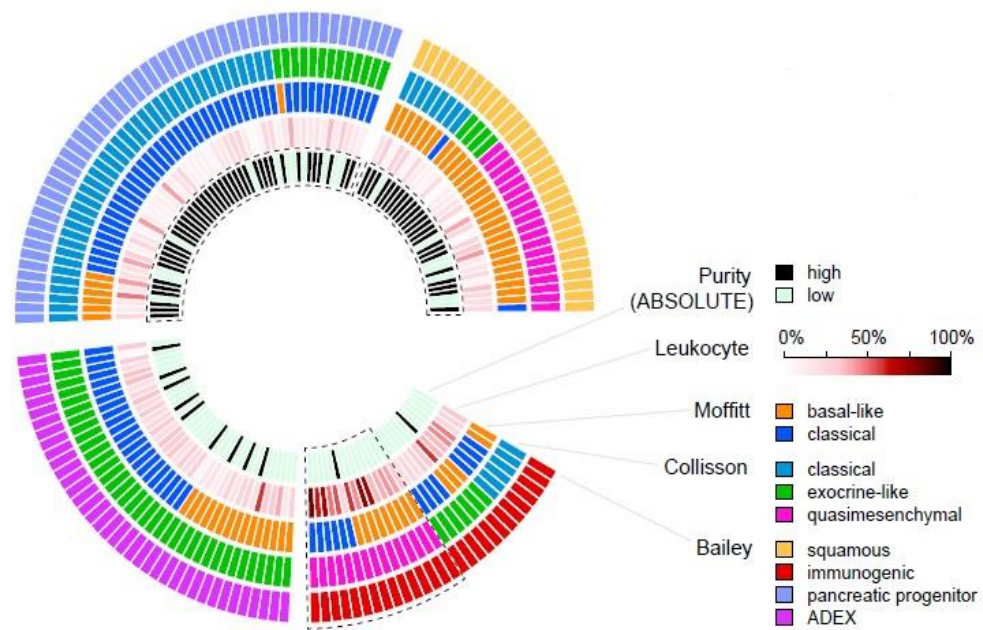


**Figure c. The main classifications of PDAC subtypes and impact of the purity on the molecular analysis<sup>16</sup>.**

The squamous subtype was determined to be an independent prognostic factor for poor survival, with the shortest median survival time of 13.3 months linked with survival times of 30.3, 25.6 and 23.7 months for the three other subtypes (Figure d)<sup>18</sup>.

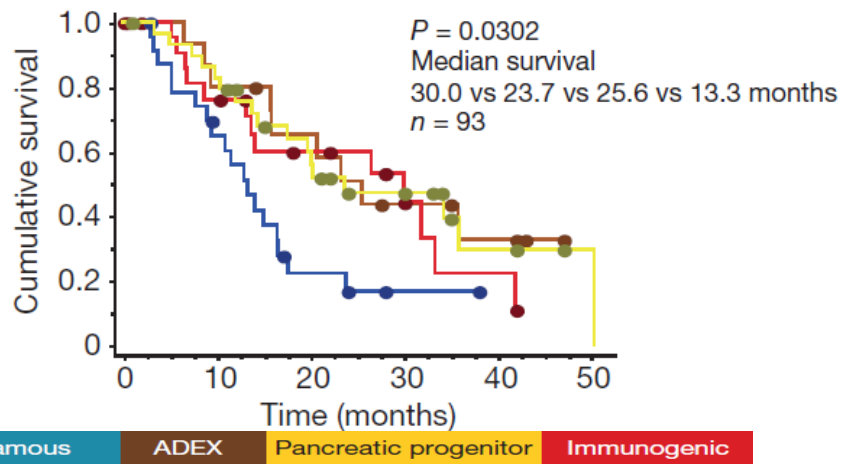


**Figure d. Kaplan–Meier analysis of patient survival stratified by class<sup>18</sup>.**

Predictive biomarkers often identify the molecular targets of relevance to use for specific anticancer drugs, and accordingly, molecular subtypes could represent promising predictive biomarkers. For example, the classical PDAC cell lines are more dependent on KRAS than QM-PDA cell lines, suggesting that KRAS-directed therapy might have the greatest efficacy against classical PDAC. Moreover, QM-PDA cell lines have been shown to be more sensitive to gemcitabine than classical subtype cell lines, which are more sensitive to erlotinib <sup>17</sup>. These results further establish phenotypic differences between the classical and QM-PDA subtypes and also that the kind of treatment changes in different PDAC classes. Therefore, the current practice of combining these drugs may increase toxicity without increasing efficacy for many patients. Sensitivity of cancer cells to drugs depends on a multiplicity of genomic and epigenomic variables <sup>22</sup>. Thus, a panel of genes could help to monitor specific subtype treated-patients and determine biomarkers that predict the likely course of the disease in a defined clinical population under specific treatment conditions <sup>23</sup>. Subtyping PDAC has opened a door

towards improved understanding of tumour biology, which would help to develop lines of targeted chemotherapies <sup>24</sup>.

#### **1.4 The rational of this thesis**

Pancreatic cancer remains one of the most lethal malignancies. While effective targeted therapies are now available for lung and colorectal cancers, no effective targeted therapy has been identified for PDAC. RAS and RAS-related proteins are often deregulated in cancers, leading to increased proliferation, invasion and metastasis. Of the Ras family of GTPases, *KRAS* is mutated in about 90% of human PDAC. The majority of *KRAS* mutations affect key aminoacidic residues, which are necessary for its GTPase activity <sup>25</sup>. The most frequent mutations affect: glycine-12 (G12), glycine-13 (G13), or glutamine-61 (Q61). These mutations render RAS persistently GTP-bound and constitutively active independently from extracellular stimuli, resulting in overactivation of effector signalling pathways, including the MAP Kinase pathway. (**Figure e**).

Unfortunately, *KRAS* is considered virtually “undruggable”, and no compound that targets *KRAS* directly has reached the clinic to date <sup>25</sup>.

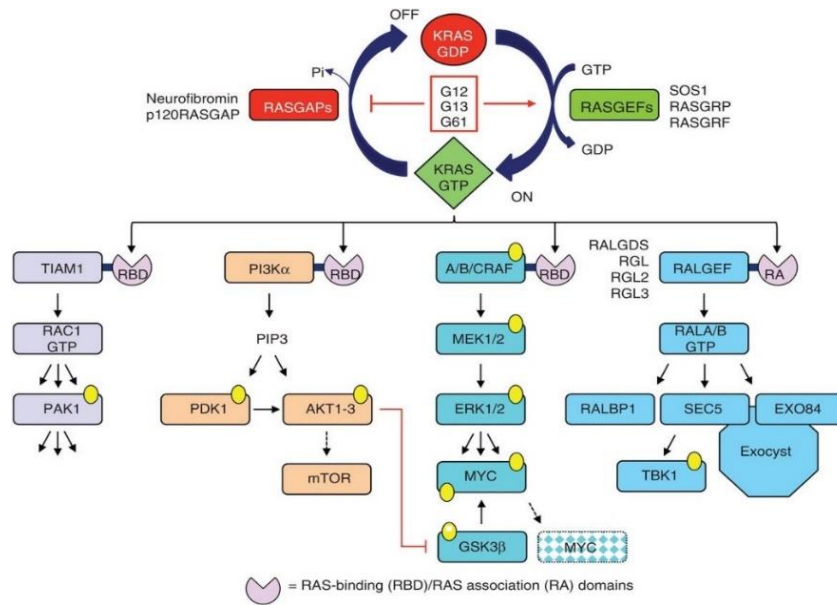


**Figure e. KRAS regulation and effector signalling** <sup>26</sup>.

Consequently, much of the past and current efforts have centred on indirect strategies <sup>26</sup> (**Figure f**). Currently, there are different inhibitors under clinical evaluation: 22 Raf inhibitors, mitogen-activated protein kinase/Erk kinase (MEK), and/or extracellular signal-regulated kinase (ERK) ([www.clinicaltrials.gov](http://www.clinicaltrials.gov)). Similarly, 43 inhibitors of the class I phosphoinositide 3-kinase (PI3K) lipid kinases and their downstream targets, serine/threonine kinase AKT and mammalian target of rapamycin (mTOR), are currently under clinical evaluation.

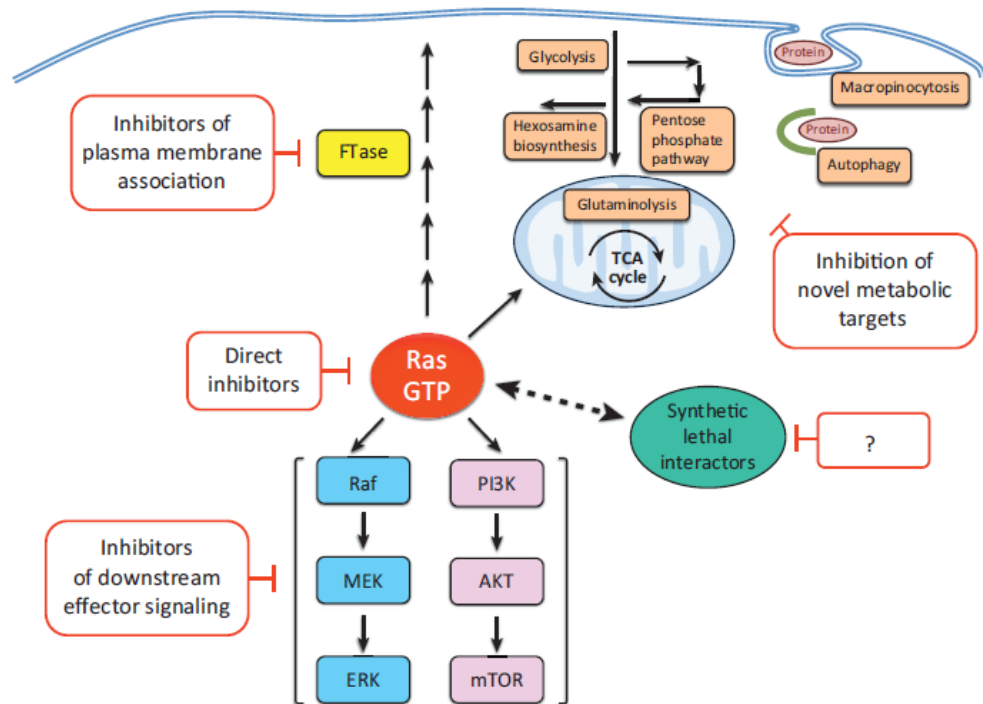


**Figure f: Anti-Ras drug discovery** <sup>27</sup>.

However, the complexity of signalling pathways suggests that hitting a single point along a cascade will be difficult, as this is usually associated to disruption of negative feedback loops that cause index pathway reactivation or switch to parallel pathways to sustain cell growth. For this reason, the combinatorial block of several downstream targets could be a potential strategy to synergistically inhibit tumor growth and delay resistance.

The aim of this thesis is to decipher the mechanisms of resistance to MEK inhibition in PDAC. This study has two principal goals: the first is to propose a molecular marker of prognosis to be used in the classification of PDAC patients; the second is to find a putative combinatorial strategy to overcome MEK inhibition resistance in pancreatic cancer.

## **2 MATERIALS AND METHODS**

### **2.1 Materials**

#### **Human pancreatic cancer cell lines and organoids: culture conditions**

Four cell lines were purchased from ATCC (American type culture collection, USA), PANC-1, Hs766T, HPAF-Three 2D cell lines (hF2, hT1 and hM1a) have been established from pancreatic organoids models in David Tuveson laboratory of the Cold Spring Harbor Laboratory Cancer Center, USA. Organoids were established from resected PDAC specimens and maintained in human complete medium<sup>28</sup>. PANC-1, Hs766T, HPAF-II, and HEK293 cells were grown in DMEM supplemented with 10% fetal bovine serum, 1% of 200Mm L-Glutamine, 1% of 10,000 units Penicillin-10mg/ml Streptomycin (Sigma-Aldrich, UK). hF2, hT1, and hM1a were grown in RPMI supplemented with 10% fetal bovine serum, 1% of 200Mm L-Glutamine, 1% of 10,000 units Penicillin-10mg/ml Streptomycin (Sigma-Aldrich, UK).

#### **Targeted therapy drugs**

Trametinib (GSK1120212) is an orally bioavailable inhibitor of mitogen-activated protein kinase kinase (MEK/MAPK/ERK kinase) with potential antineoplastic activity. It was purchased from Selleckchem, dissolved in dymethyl sulfoxide (DMSO) to produce a 10mM, 5mM and 1mM stock solution and stored at -80°. Vorinostat is a histone deacetylase (HDAC) inhibitor purchased from Selleckchem and dissolved in DMSO as a 10mM stock solution and stored at -80°C. The Dovitinib is a selective FGFR inhibitor (FGFR1/3); it was

purchased from Selleckchem, dissolved in DMSO as a 10mM stock solution and stored at -80°C.

## 2.2 Methods

### Cell line maintenance

Cells were cultured in 10 or 15cm<sup>2</sup> tissue culture dishes (Thermo scientific) and Organoids in 24 well tissue culture plates (Corning) at 37°C in a humidified atmosphere of 5% CO<sub>2</sub> and procedures were carried out in sterile conditions in Class II biological safety cabinets. Cells were routinely passaged by removing the medium and by gently washing once with sterile PBS. Following PBS removal, cells were detached by incubation with 2-5mL of Trypsin-EDTA (volume of trypsin was adjusted to the dimension of the cell culture dish) for 3-5min at 37°C. After detachment, complete medium was added to the cells in order to stop the action of the trypsin (volume of medium was equal to the amount of trypsin used). Cells were then collected and centrifuged at 1000rpm for 5min. The resulting cell pellets were resuspended in fresh medium before reseeding into new culture dishes at a ratio of 1/3 to 1/5 according to the cell line. For the passaging of organoids, the medium was removed and the matrigel domes containing organoids were collected in an ice-cold 15 ml Falcon tube containing in a final volume of 10 ml of Splitting Media. Then the organoids were centrifuged at 100 RCF for 5' at 4°C and then the media was aspirate off until 1.8 ml to break up organoids using a fire-polished pipette by pipetting 10 times. After the refill of the Falcon tube to 10 ml with ice-cold splitting medium, organoids were centrifuged again at 100 RCF for 5' at 4°C. The resulting pellet was resuspended in ice-cold matrigel considering 50 ul per new well of 24-well plate. After a 15 minutes incubation at 37°C the human complete medium was added. It is worth to add that all the used cell lines were routinely tested for Mycoplasma using MycoAlert mycoplasma detection kit from Lonza.

### **RNA extraction and real time quantitative polymerase chain reaction (RT-qPCR)**

RNA was extracted using Trizol reagent, that is a monophasic solution of phenol and guanidinium isothiocyanate that simultaneously solubilizes biological material and denatures protein. After solubilization, the chloroform's addition causes phase separation and RNA remain in the aqueous phase.

$1 \times 10^5$  to  $5 \times 10^5$  cells were plated in a six-well plate or a 10 cm dish. After 24 hours cells were treated with trametinib. RNA was extracted using Trizol® Reagent method (Life Technologies) and according to the manufacturer's protocol. The concentration was determined using the NanoDrop 2000 Spectrophotometer. 1µg of extracted RNA was transcribed reversely into c-DNA by using high capacity cDNA reverse transcription kit (Life Technologies). Real time qPCR was performed in duplicate or triplicate using 20ng of cDNA for the genes expression analyses and 10ng for micro RNA expression analyses. TaqMan and Sybergreen dyes were used as reporters and the applied biosystem 7900HT RT-PCR machine was employed for PCR amplification. PCRs were done in a 20µL reaction volume. The following protocol was used: initial incubation at 95°C for 10 minutes followed by 45 cycles at 95°C (15 seconds) and 60°C (1 minute). Cycle Threshold (CT) values, used to calculate the changes in gene expression, and were generated by the Applied Biosystems SDS software. Gene expression analysis (CT method and statistical analysis) was performed with Excel.

**Table 2: List of probes used during this project.**

| <b>Probes</b> | <b>Identification code</b> | <b>Suppliers</b>        |
|---------------|----------------------------|-------------------------|
| ErbB3         | Hs00176568_m1              | Life technologies Italy |
| HNF4a         | Hs00230853_m1              | Life technologies Italy |
| SNAI1         | Mm00441533_g1              | Life technologies Italy |

|           |               |                         |
|-----------|---------------|-------------------------|
| ZEB1      | Mm00495564_m1 | Life technologies Italy |
| FGFR3     | Hs00997400_g1 | Life technologies Italy |
| EphA4     | Hs00953172_m1 | Life technologies Italy |
| miRNA-99a | 000435        | Life technologies Italy |
| miRNA-100 | 478224_mir    | Life technologies Italy |
| DUSP6     | Hs04329643_s1 | Life technologies Italy |
| SPRY4     | Hs01935412_s1 | Life technologies Italy |
| HPRT1     | Hs02800695_m1 | Life technologies Italy |

## Western blot analysis

### Protein extraction

Cells were washed twice with ice-cold DPBS buffer. The cells were scraped with DPBS and centrifuged at 1200 rpm for 5 min to obtain a pellet. Cell signaling Lysis buffer containing fresh protease inhibitor and phosphatase inhibitor (Roche, UK), was added to the cells then gently mixed and put on a rotor at 4 degrees for 45 minutes to one hour. Samples were then pelleted by centrifugation for 15 minutes at 4°C (14000rpm). The total cell lysate (supernatant) was placed in a fresh tube and stored at -80°C.

### Protein quantification

Proteins were quantified using the colorimetric RC-DC protein assay from Bio-Rad Laboratories. Protein quantification is based on the use of three reagents: A, S, and B. A 1:8 dilution of each protein sample was prepared in order to quantify each sample in duplicate. A mix of reagent A and S was also prepared (20ul of reagent S with 1ml of reagent A) and 25uL of this mix was added in each well of a flat-bottom 96 well plate. Pre-diluted protein assay standards (Bovine Serum Albumin, Sigma-Aldrich) curve was used to calculate the protein concentration of the samples under investigation. 10ul of each standard (125ug/mL, 250ug/mL, 500ug/mL, 750ug/mL, 1000ug/mL,

1500ug/mL and 2000ug/mL) or unknown sample replicates were pipetted per well. 200uL of reagent B was then added to each well and the content of the plate was mixed on a shaking platform for 15min at RT. Absorbance (OD) was measured at 750nm with the Synergy Biotek (Biotek). The average absorbance measurement of the blank sample was subtracted from the all the measurements of both standard and unknown samples. A standard curve was then prepared by plotting the average absorbance value of each standard vs. its concentration ( $\mu\text{g/mL}$ ). The standard curve generated can be used to calculate the protein concentration of each unknown sample.

### **Immunoblotting**

The proteins were then separated based on molecular weight by gel electrophoresis and transferred to blotting membrane. Membranes were then incubated with labels primary antibodies and the signal was detected using anti-mouse or anti-rabbit secondary antibodies. 20-50ug of protein from samples prepared as described were centrifuged for 10 seconds, heat-denatured for 15min at 95°C in NuPAGE LDS *Sample Buffer (4X)*, 10% b-mercaptoethanol (Life Technologies) and loaded on a 4-12% Bis-Tris NuPAGE gel (Novex, Pre-cast gels, Life Technologies). 20x MOPS (Sigma-Aldrich) running buffers were diluted to 1x with distilled water and were used for protein electrophoresis at 120 Volts. The protein marker spectra multicolour broad range ladder (Thermo scientific) and Precision plus protein standards (Biorad) were used as a molecular weight protein standard. Proteins were subsequently transferred to polyvinylidene difluoride membranes (Immobilon®-P transfer membrane; Millipore), which had been previously activated by immersion in Methanol (VWR) for 1 min. The transfer buffer was prepared with a 1:10 dilution of a 10x Tris-Glycine buffer [30.3g Tris-Base (Sigma-Aldrich) and 144.1g Glycine

(Sigma-Aldrich)] in distilled water and 20% Methanol. Proteins were transferred at 400mA for 1.5 hour at RT and membranes were subsequently blocked for 1h at room temperature in blocking buffer containing 5% BSA (Sigma-Aldrich) in 1x TBS, 0.1% Tween-20 (Sigma-Aldrich) or 5% milk in 1x TBS, 0.1% Tween-20 (Sigma-Aldrich). All primary antibodies were incubated overnight at 4°C. The antibody dilutions were kept at -20°C. Anti-rabbit or mouse IgG, HRP-linked Antibodies (Cell Signalling Technologies) were used to detect the primary antibodies binding (dilutions ranging from 1:1000 to 1:5000 depending on the primary antibody used). Membranes were washed three times in 1xTBS-0.1% Tween-20 buffer for 10min following incubation with primary and secondary antibodies. The antibody binding to the protein of interest was detected by enhanced chemiluminescence (ECL system, Amersham) and ECL substrate for western blot (Euroclone) were develop on autoradiography carestream Biomax film, Kodak (Sigma Aldrich). Reprobing of membranes with different antibodies specific for proteins with similar molecular weight (e.g. phosphorylated and total proteins) was performed by stripping the original bound antibody from the membrane with 8-15 min incubation with the Restore™ PLUS western blot stripping buffer (life technologies). Alternatively, protein lysates were re-analysed by western blotting in the exact same conditions.

### **Cell titer Glo assay**

The CellTiter-Glo® Luminescent Cell Viability Assay is a homogeneous method to determine the number of viable cells in culture based on quantitation of the ATP present, which signals the presence of metabolically active cells. After 72 hours of trametinib/Vorinostat/Dovitinib treatments we used CellTiterGlo method to determine the EC50 as indicated by the supplier (Promega).

EC50s are defined as the concentrations of drug that result in 50% cell survival compared with untreated cells. The EC50 curves were made using Prism Graphpad.

### **Long-term viability assay**

Cells were plated  $1 \times 10^4$  to  $50 \times 10^4$  in six well-plate. They were allowed to attach to the plate and were treated after 24 hours with gradual concentration of trametinib. The concentrations were: 1nM, 5nM, 10nM, 50nM, 100nM. Trametinib was diluted in DMSO, so we used as vehicle cell treated with normal medium containing 0.1% DMSO. Each treatment point was plated in duplicate, and every experiment were made three times. The plates were then stained with crystal violet (0.5% w/v) prepared in 95% Ethanol and allowed to dry at room temperature. Cells were then solubilized using acetic acid and a multiplate reader (Synergy 4, Biotek) was used to determine the absorbance at 750 nM.

### **Phospho-receptor tyrosine kinase array**

We used R&D Systems™ Human Phospho-Receptor Tyrosine Kinase (RTK) Array Kit (Catalog # [ARY001B](#)), which is a screening tool designed to simultaneously detect the relative phosphorylation of 49 different RTKs. This kit eliminates the need for numerous immunoprecipitation (IP) and/or Western blot experiments. PDAC cell lines were continuously treated with trametinib for 72 hours, and 1 week prior to harvest. The drug was renewed every 72 hours. At the end of the treatment, media was removed, cells were rinsed with ice cold PBS, then scraped in cold PBS and centrifuged at 1200 rpm for 10 minutes at 4°C. Cells were lysed with the lysis buffer 17 from the R&D Proteome Profiler Arrays Human phospho-RTK array (R&D systems, Minneapolis, MN, Catalog No. ARY001). These arrays have

immobilized specific antibodies for individual RTKs spotted in duplicate on a filter the size of a microscope slide. The RTKs are recovered from a single cell extract and their activation revealed by immunostaining for phosphor-tyrosine. Identical amounts of total protein (300 micrograms) from extracts of PDAC cells were incubated with the antibody arrays overnight at 4 ° C and developed according to manufacturer's instructions with the chemiluminescent detection reagents furnished by the supplier. Quantitation of the arrays was performed using QuantityOne software.

### **Immunohistochemistry**

Paraffin-embedded tissue block were cut into 3 µm sections and mounted on adhesion microscope glass slides. For immunohistochemical staining, sections were stained using Leica Bio-System BOND III with the abovementioned antibodies. Slides were deparaffinized twice in xylene for 5 minutes and rehydrated through graded ethanol solutions to distilled water. Antigen retrieval was performed by heating sections in citrate buffer, ethylenediaminetetraacetic acid buffer, or enzymatically with proteinase K. Inactivation of endogenous peroxidase activity was obtained by incubating sections in 3% H<sub>2</sub>O<sub>2</sub> for 15 minutes. Localization of bound antibodies was performed with a peroxidase-labelled streptavidin-biotin system (DAKO, LSAB2 Kit) with 3, 3'-diaminobenzidine as a chromogen. Appropriate positive controls for each antibody were run concurrently and showed adequate immunostaining.

**Table 3.** List of antibodies used for western blot and immunohistochemistry.

| Antibody | Clones/Cat | Dilution | Suppliers |
|----------|------------|----------|-----------|
|----------|------------|----------|-----------|

|                       |                     |        |                 |
|-----------------------|---------------------|--------|-----------------|
| Zeb1                  | ab203829            | 1:1000 | Abcam           |
| ErbB3                 | D22C5/12708         | 1:1000 | Cell signalling |
| E-cadherin            | NCH-38              | 1:1000 | Novocast        |
| Vimentin              | V9                  | 1:1000 | Dako            |
| b-Actin               | 4967S               | 1:5000 | Cell signalling |
| p-Erk1/2              | 9101S               | 1:1000 | Cell signalling |
| Erk1/2                | 9102S               | 1:1000 | Cell signalling |
| p-Akt                 | D5G4/#12178         | 1:1000 | Cell signalling |
| Akt                   | 9272S               | 1:1000 | Cell signalling |
| Vinculin              | 4650s               | 1:1000 | Cell signalling |
| P-FGFR3 (Y724)        | EPR2281(3)/AB155960 | 1:1000 | Cell signalling |
| P-FRS2-alpha (Tyr436) | 3861                | 1:1000 | Abcam           |
| FGFR3                 | EPR2305(3)/ab137084 | 1:1000 | Abcam           |
| c-MYC                 | Y69/ab32072         | 1:1000 | Abcam           |
| EphA4                 | ab5389              | 1:1000 | Abcam           |

### RNA sequencing

RNA was extracted from cell cultures or freshly isolated tissues using TRIzol (Invitrogen), followed by column-based purification with the PureLink RNA Mini Kit (Ambion). The quality of purified RNA samples was determined using a Bioanalyzer 2100 (Agilent) with an RNA 6000 Nano Kit. RNAs with RNA Integrity Number (RIN) values greater than 7.5 were used to generate sequencing libraries using the TruSeq Stranded mRNA Kit (Illumina) per manufacturer's instructions. Sequencing libraries were run at Eurofinsgenomics using an Illumina HiSeq2000. Sequence pairs were mapped to either the human (GRCh38) or the mouse (GRCm38) reference genome, using the STAR 2.5.3a software <sup>29</sup>. Raw counts were normalized using

DESeq2 v1.18.1 rlog function <sup>30</sup>. Gene differential expression analysis was performed using the limma v3.34.2 R package <sup>31</sup>.

### **Connectivity Map Query.**

For CMap analysis, the 300 most significantly up- and downregulated genes based on log ratio of gene expression of MEK-treated compared to vehicle-treated tumors were identified. The list of genes from both the human and the mouse experiment that was used for the CMap query (<https://www.broadinstitute.org/connectivity-map-cmap>) is available as **Supplementary Table 1**. Each signature was queried against the CMap using the gene set enrichment analysis algorithm described by Lamb et al <sup>32</sup>.

### **Statistical Analysis and Data mining**

For data mining and pancreatic cancer subtypes stratifications we used two different datasets. The first dataset represents the PACA-AU cohort of the ICGC consortium, downloaded from the supplemental material of the corresponding publication <sup>18</sup>. This dataset contains normalized expression values (TMM normalized using edgeR Bioconductor package, converted to CPM and log2 transformed) of 96 pancreatic cancer patients; for subtypes stratification, z-scores were calculated for each gene. Associated clinical data were downloaded from <https://dcc.icgc.org/releases/current/Projects/PACA-AU>. The second dataset represents the TCGA-PAAD cohort, downloaded from <http://firebrowse.org/?cohort=PAAD>, which consists of the RNA-Seq gene expression profile of 178 pancreatic cancer patients. According to other publications that disputed the purity of some samples, we restricted the number to 148 assured samples. The grouping of the samples in Bailey's and Moffitt's subtypes <sup>20</sup> was performed with the GSVA Bioconductor package with the same options as above. The

gene sets used for the stratification were retrieved from the original publications. Unless indicated, all the p-values refers to Wilcoxon rank-sum test.

## RESULTS AND DISCUSSION

### Subtyping of human PDAC cell lines

To identify mechanisms of resistance to MEK inhibition in PDAC, we selected 6 human PDAC cell lines all bearing mutations of *KRAS* (**Table 2**). Three of those 2D cell lines were established from human pancreatic cancer organoid cultures (hM1a, hT1, hF2), which were originally derived in the laboratory of David Tuveson and described in Boj et al <sup>28</sup>. Based on characteristics of neoplastic cells, PDAC can be reliably classified as squamous/quasi-mesenchymal/basal-like or pancreatic progenitor/classical <sup>33</sup>. Therefore, we performed RNA sequencing (RNA-seq) and applied the Bailey classification <sup>18</sup> to subtype the 6 PDAC cell lines as pancreatic progenitor (PP) (HPAF-II, hF2, hM1a) or squamous (Sq) (hT1, PANC1, Hs766T) (**Figure 1a**). In keeping with the mRNA-based classification, Sq and PP cell lines showed differential expression of known markers of epithelial- (ERBB3, HNF4a, E-Cadherin) and mesenchymal-cell state (ZEB1, Vimentin, SNAIL). High expression of the transcription factor ZEB1 and low ERBB3 expression were observed at protein level in the squamous cell lines (Figure 1b), which is in line with previous report <sup>17</sup>. High protein expression of the cytoskeleton protein Vimentin, a known mesenchymal marker, was detected in 2 (hT1 and PANC1) of the 3 squamous cell lines. Conversely, pancreatic progenitor cell lines presented high protein expression of E-Cadherin and ERBB3, but low to no detectable expression of the mesenchymal markers ZEB1 and Vimentin (Figure 1b). When looking at mRNA expression of *HNF4a*, *ERBB3*, *ZEB1*, and *SNAIL*, we only found a trend towards significance for higher expression of *HNF4a* and *ERBB3* in PP compared to Sq cell lines (Figure 1c). The methylation status and the expression of pancreatic

transcription factors were also reported to distinguish the pancreatic progenitor from the squamous subtype<sup>18,34</sup>. Hypomethylation of *PDX1* and the associated increase in gene expression, for example, are observed in the PP subtype<sup>18</sup>. In line with this, our PP cell lines displayed increased nuclear immunostaining of PDX1 and reduced cytoplasmic expression of the squamous marker Cytokeratin 5 (CK5, Figure 1d). Taken together, our data clearly showed that 6 PDAC cell lines could be reliably classified as either pancreatic progenitor or squamous. Henceforward, we will use interchangeably the terms pancreatic progenitor/classical and squamous/basal-like.

**Table 2. Mutations of PDAC “driver” genes in the 6 cell lines used in the study.**

| Cell lines | KRAS   | TP53    | CDKN2A(P16) | SMAD4 |
|------------|--------|---------|-------------|-------|
| hM1a       | p.G12D | p.R175H | WT          | WT    |
| Hs766T     | p.Q61H | WT      | WT          | HD    |
| hT1        | p.G12V | R213*   | HD          | LOH   |
| hF2        | p.G12V | WT      | WT          | HD    |
| HPAF-II    | p.G12D | p.P151S | p.R29fs*9   | WT    |
| PANC-1     | p.G12D | p.R273H | HD          | WT    |

NOTES: p., protein sequence; \*, stop gain, WT, wild-type sequence; fs, frameshift; HD, homozygous deletion; LOH, loss of heterozygosity.

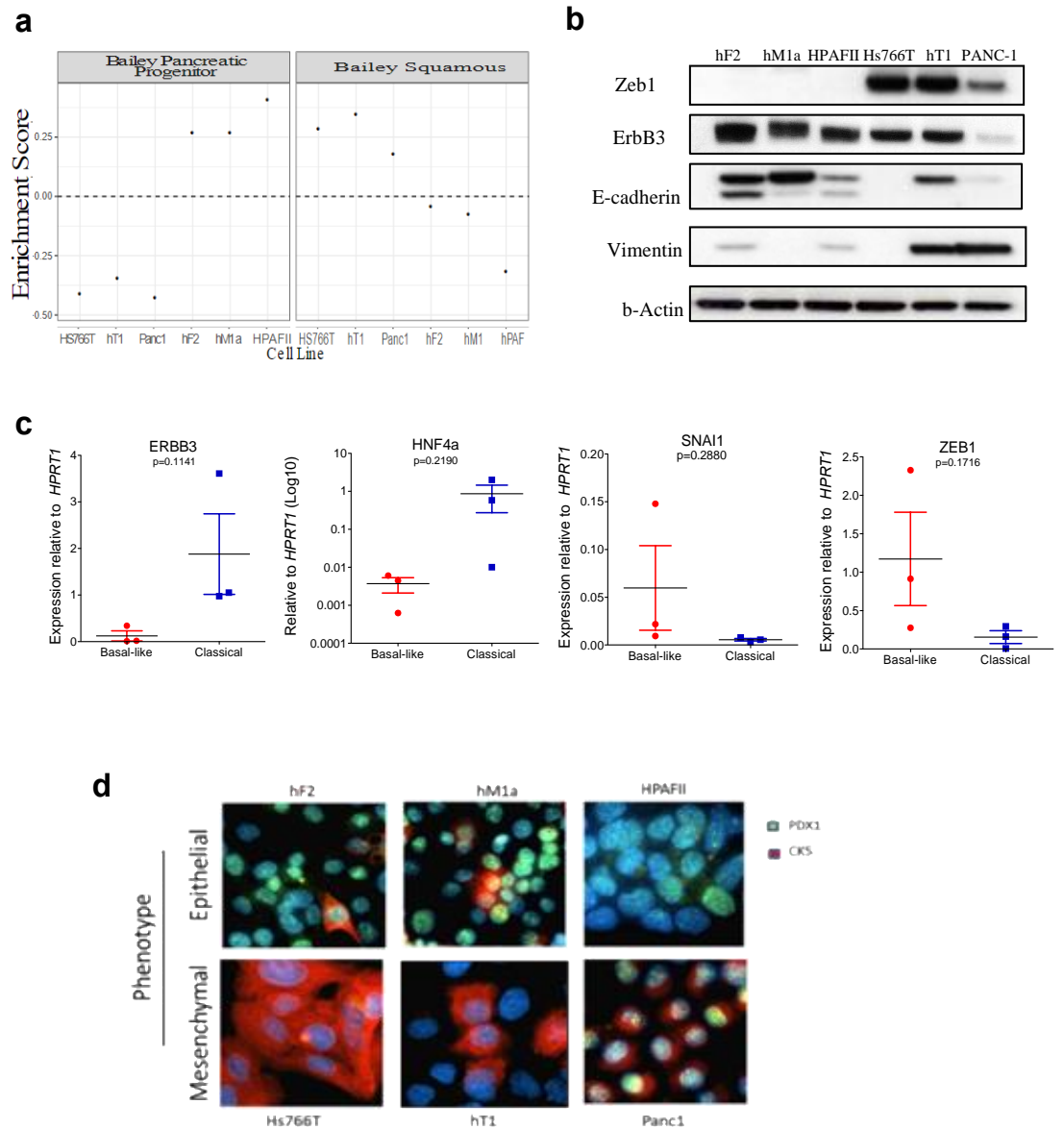


**Figure 1. Subtyping of PDAC cell lines.** **a** Enrichment score of the signatures of Pancreatic Progenitor and Squamous subtypes as defined in Bailey et al.<sup>18</sup>. Signatures scores for each individual cell lines are reported. **b** Immunoblot analysis of selected epithelial (ErbB3, E-cadherin) and mesenchymal (ZEB1, Vimentin) markers in whole lysates from individual cell lines. **c** mRNA levels of indicated genes in basal-like (n = 3) and classical (n = 3) cell lines. Levels of individual genes were normalized to *HPRT1*. Data are displayed as scatter dot plot with average and standard

error of the mean (SEM). p values calculated with Student's t test. **d** Representative immunofluorescence staining for PDX1 (green) and CK5 (red) in 6 PDAC cell lines. Nuclei are stained with DAPI (blue). Images were taken at 100X magnification.

### **MEK inhibition has different efficacy in PDAC cell lines**

Previous studies have demonstrated that PDAC subtypes exhibit different sensitivity to both chemotherapy and targeted agents<sup>17,35</sup>. Therefore, we sought to assess whether our subtyped cell lines showed differential sensitivity to the inhibition of MAP kinase with the allosteric MEK1/2 inhibitor trametinib (MEKi). PDAC cells were challenged with different doses of MEKi for either 72 hours or 1 week of continuous treatment. Basal-like cell lines were generally found to be more resistant to both short- and long-term trametinib treatment compared to classical cell lines (**Figure 2a, 2b, Table 3**). To explore the biochemical adaptive changes to MEKi in PDAC, we treated PDAC cell lines with subEC50 concentrations of MEKi for 72 hours and 7 days. Short-term (72hours) MEKi treatment effectively inhibited phosphorylation of the MEK1/2 target (ERK1/2) (Figure 2c). No compensatory hyperphosphorylation of AKT was consistently observed in PDAC cell lines. Despite the continuous presence of the drug, re-activation of ERK1/2 was observed at one week of treatment suggesting the engagement of compensatory pathways to overcome the blockade and to maintain the index oncogenic signalling output (Figure 2c).

**Table 3. EC50 concentration of 72 hours MEKi treatment of PDAC cell lines**

|           | <b>Cell lines</b> | <b>EC50</b> |
|-----------|-------------------|-------------|
| SENSITIVE | hM1a              | 1.34 nM     |
|           | Hs766T            | 2.85 nM     |
|           | hF2               | 4.54 nM     |
|           | HPAFII            | 4.80 nM     |

|           |        |              |
|-----------|--------|--------------|
| RESISTANT | hT1    | 148.8 nM     |
|           | PANC-1 | 9.24 $\mu$ M |

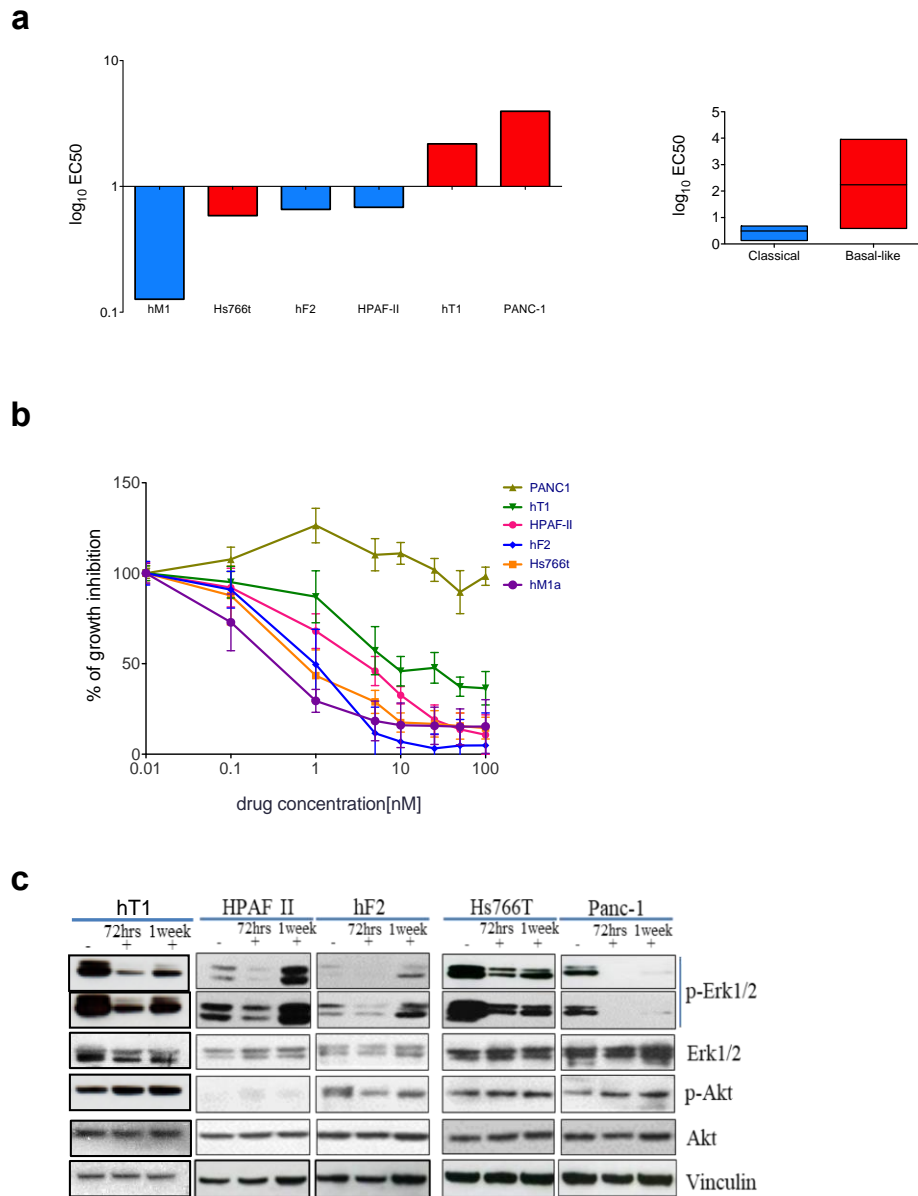


**Figure 2. MEK inhibitor efficacy in PDAC cell lines.** **a** Half-maximal effective concentration (EC<sub>50</sub>) in log<sub>10</sub> of drug concentration is plotted for each cell line tested. In blue, classical cell lines; in red, basal-like cell lines. Floating bars plot on the right display the same data after grouping PDAC subtypes. **b** Dose-response curves of PDAC cell lines treated with increasing concentration of the MEK inhibitor trametinib for one week. Data are representative of three technical replicates for each cell line. Errors indicate

standard deviation. **c** Immunoblot analysis of selected effectors of MAP Kinase (ERK1/2) and PI3K/AKT (AKT) pathways in PDAC cells lines following 72 hours and 1 week of MEKi treatment. Short and long exposures are reported for phosphor-ERK1/2. Vinculin was used as loading control.

### **MEK inhibition induce the kinome reprogramming in PDAC**

Upon treatment with targeted agents, pathway reactivation represents the most common mechanism of resistance. Pathway reactivation might consequence either from alterations of the drug targets or engagement of upstream/downstream effectors of the index drug-inhibited oncogenic signalling pathway<sup>36</sup>. Of those, activation of Receptor-Tyrosine Kinases (RTKs) is the well-described mechanism of resistance to targeted agents<sup>36</sup>. Therefore, to investigate whether MEK inhibition resulted in the reprogramming of the Receptor-Tyrosine (RT-) Kinome in PDAC, we subjected the 6 PDAC cells treated with vehicle or MEKi for 2 and 7 days to unbiased RNA-seq. Following 2 days of treatment, increased transcriptional ratio (FC>2) ranged from 2% (HPAF-II) to 10% (Hs766t), while transcripts downregulation (FC<2) ranged from 1% (HPAF-II) to 3.5% (hM1a) (**figure 3a**). Following 7 days of continuous treatment, transcripts upregulation (FC>2) ranged from 4% (hF2, PANC1, HPAF-II) to 13% (Hs766t), whereas decreased transcriptional ratio (FC<2) ranged from 2% (HPAF-II) to 7% (Hs766t) (Figure 3a). No specific pattern of global transcriptome reprogramming could be identified between PDAC subtypes. Taken together, this data shows that MEKi has effect of different amplitudes on the transcriptomes of PDAC cell lines, and that bigger effects are seen after 7 days of drug challenging rather than shortly after the start of the treatment. The presence of mismatching time points in our RNA-seq analysis provides the opportunity of identifying shared and divergent transcriptional responses to short- and long-treatments. Global responses might either entirely reflect adaptation to the environmental cue (the treatment) or include stochastic components, i.e. deregulated genes during stress without any evident association to the specific environmental cue. At biochemical level, we observed that the pathway is effectively inhibited at two days

while recovering at 7 days of treatment. Therefore, we reasoned that considering deregulated genes that are shared between the two different time points might help excluding stress-related responses as well as likely identifying processes that have direct functional relevance to the specific perturbation.

Examination of the RT-kinome nominated 3 proteins (*ROS1*, *FGFR3*, and *MYD88*) as the most induced transcripts across the 6 cell lines (Figure 3b, **Supplementary Table 1**). Of these, *ROS1* and *FGFR3* are *de facto* RTKs, while *MYD88* encodes for an intracellular adaptor protein that is involved in NF-kappa-b signalling<sup>37</sup>. *ROS1* encodes for a receptor tyrosine kinase that undergoes genomic rearrangements of the 3' region in a variety of cancers<sup>38</sup>. These rearrangements create chimeric products retaining the kinase domain of ROS1 and are implicated in driving tumorigenesis as well as in the response to targeted agents (e.g., crizotinib)<sup>38</sup>. *FGFR3* is a member of the FGFRs family, which encompasses 4 highly conserved of tyrosine kinase receptor to which bind a total of 18 FGFs<sup>39</sup>. The role of aberrant FGFR signalling is well established in several malignancies (e.g., lung and bladder cancer)<sup>40 41</sup>, but its role in PDAC has been largely neglected so far. Of note, one of the most upregulated genes following MEKi encodes for EPHA4, a receptor that has been reported to interact with FGFR3 at cytoplasmic level to engage downstream signalling molecules (e.g., FRS2) that lead to MAP kinase activation<sup>42</sup>. To validate the kinome reprogramming in a more physiological setting, we leveraged RNAseq from mouse isografts treated with either vehicle or trametinib for 7 days, which was already available in our lab (Figure S1). In line with the *in vitro* experiment, *Fgfr3* and *Ros1* were amongst the most upregulated genes following MEKi *in vivo*.

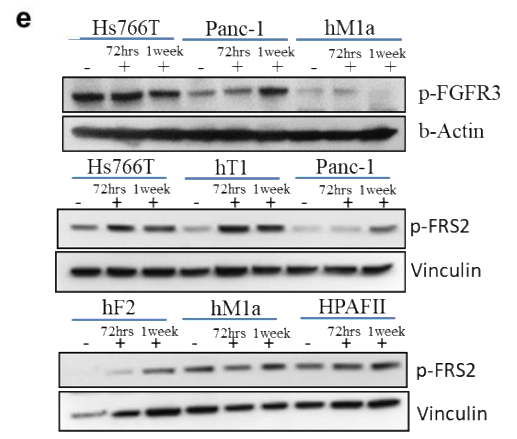
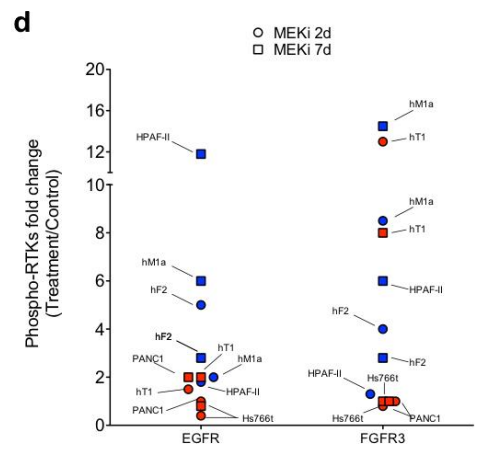
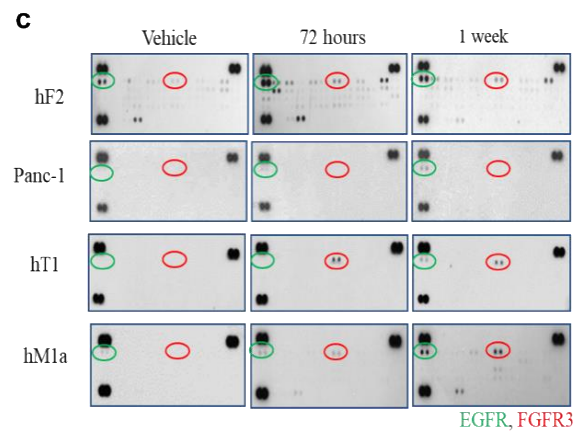
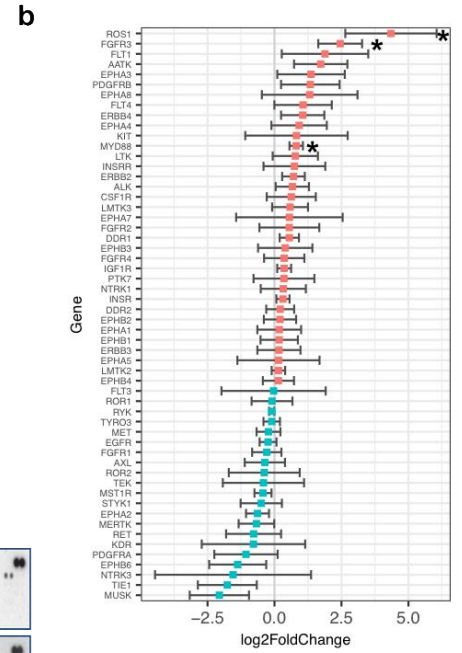
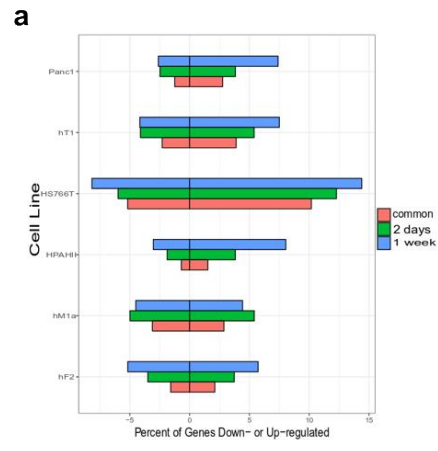


**Figure 3. MEKi induce kinome reprogramming in PDAC cell lines. a** Percentage of upregulated and downregulated transcripts ( $FC \geq 2$ ) in the six cell lines following trametinib treatment. The total number of detected transcripts is 19,837; percentage of genes deregulated after 2 days (green), 7 days (blue), and genes deregulated both at 2 and 7 days is reported. **b** DESeq2 analysis comparing trametinib treatment with vehicle control. Shown are differentially expressed RTK genes ( $\log_2$  fold change). Upregulated transcripts are highlighted in red, while downregulated genes are highlighted in blue. \*,  $p < 0.05$  by Student's t test. **c** Representative phospho-RTKs arrays of human PDAC cell lines treated with subEC50 concentration of MEKi for 72 hours and 1 week. Signals referring to EGFR and FGFR3 are indicated by green and red circles, respectively. **d** Quantification of changes in the level of phospho-EGFR and phospho-FGFR3 after treatment of the 6 PDAC cell lines with MEKi for 72 hours and 1 week relative to control (DMSO). Classical cell lines are indicated in blue, while basal-like cell lines are indicated in red. **e** Immunoblot analysis of phospho-FGFR3, phospho-FRS2 in whole cell lysates from cells treated with MEKi for 72 hours and 1 week. Beta-actin was used as loading control.

### **MEK inhibition induce activation of FGFR3 in human PDAC**

Increased signalling through RTKs can result from augmented expression of the receptor(s), increased level of ligands, or downregulation of negative regulators of the pathway. It is also well established that increased expression of an RTK on the cell surface does not necessarily translate into increased receptor activation. Therefore, we sought to evaluate whether MEKi in PDAC broadly resulted in activation of RTKs using commercially-available phospho-arrays for 49 individual RTKs (including ROS1 and FGFR3). Upon MEK inhibition, we observed phosphorylation of EGFR and FGFR3 in 5 and 4 of the 6 cell lines, respectively (Figure 3c-3d and **Figure S2**). Of the RTK identified, FGFR3 is the only one for which we defined a treatment-induced transcriptional response. In particular, increased phosphorylation of FGFR3 was observed in hF2, hT1, and hM1a both at 2 and 7 days of treatment (Figure 3c-d), while phospho-FGFR3 was only detected after 7 days of treatment in HPAF-II (Figure S2). No increase in the level of phospho-FGFR3 was seen in PANC1 or Hs766t upon MEK inhibition. However, independent immunoblot experiments showed increased phosphorylation of FGFR3 and its downstream effector FRS2 also in PANC1 and Hs766t (Figure 3d), thereby suggesting that activation of FGFR3 and its downstream pathway is a common biochemical response to MEK inhibition in PDAC. Differently from Ruess and colleagues<sup>43</sup>, we did not consistently observed phosphorylation of multiple RTKs upon MEKi in PDAC, which might be explained, at least in part, by differences in the experimental setup. To explore biochemical adaptation to MEKi in PDAC, we used subEC50 of the MEK inhibitor trametinib, while Ruess and colleagues interrogated RTKs activation using high doses of a different MEK inhibitor, namely selumetinib<sup>43</sup>.

## **Potential mechanisms of FGFR3 activation in PDAC upon MEK inhibition**

Our data suggest that transcriptional upregulation and activation of FGFR3 might be involved in bypass adaptive resistance to MEKi in at least a subset of PDAC. Therefore, we first sought to independently validate this finding by analysing expression of FGFR3, and its interactor EPHA4, upon MEKi both at mRNA and protein levels. In line with RNA-seq data, transcriptional upregulation of *FGFR3* was observed in 5 of the 6 cell lines at least at one treatment time-point (**Figures 4a-b**). Increased expression of *EPHA4* was evaluated only after two days of treatment and changes showed to be consistent with RNA-seq data (Figure 4c). We further validated MEKi-induced expression of FGFR3 and EPHA4 at protein levels. As expected, MYC protein levels were higher in basal-like PDAC, yet its level was reduced following treatment regardless of the subtype (Figure 4d). While increased protein expression of FGFR3 was observed in PDAC cell lines following treatment, EPHA4 levels were found to decrease upon MEKi (Figure 4d). Of note, increased expression of FGFR3 following short-term MEKi treatment was also observed in the patient' derived organoid culture hT3 (Figure 4e). Taken together, this data shows that MEKi induces expression of FGFR3 in PDAC regardless of the subtype.

FGFR3 expression is known to be regulated by two microRNAs, namely miR-99a and miR-100<sup>44,45</sup>. In line with this, oncogenic fusion involving *FGFR3* in glioblastoma results in the loss of 3' UTR of FGFR3<sup>45</sup>, thereby blocking regulation by miR-99a and enhancing expression of the chimeric product. Therefore, we sought to evaluate whether MEKi-induced FGFR3 upregulation was associated to downregulation of miR-99a and miR-100. Interestingly, levels of

miR99 ( $p=0.13$ ) and miR100 ( $p<0.01$ ) were lower in classical/PP compared to basal-like/Sq cell lines (Figure 4f). Accordingly, *FGFR3* had a trend towards higher expression in the 3 classical cell lines ( $p=0.06$ ) and was significantly enriched in the classical PDAC in patients from the TCGA cohort (Figure 4g,  $p<0.001$ ). When looking at the levels of the 2 miRNAs after MEK inhibition, we observed downregulation of miR-99a and/or miR-100 in all cell lines tested (Figure 4h-i). Activity through FGFRs is also tightly controlled by inhibitory regulators including Sprouty (SPRYs) and DUSPs proteins<sup>46-48</sup>. In particular, the Sprouty proteins antagonize FGFR-mediated MAP Kinase activation by competing with FRS2 for binding to GRB2 and the SOS complex<sup>47,48</sup>. Then, we looked at RNA-seq data for expression of DUSPs and SPRYs genes and then validated that *DUSP6* and *SPRY4* were dramatically downregulated following treatment (Figure 4j-k). Although speculative, our data suggests that activation of FGFR3 results from reduced expression of regulatory small RNAs and that signalling through FGFR3 is further exacerbated by the downregulation of negative regulators SPRY4 and DUSP6.

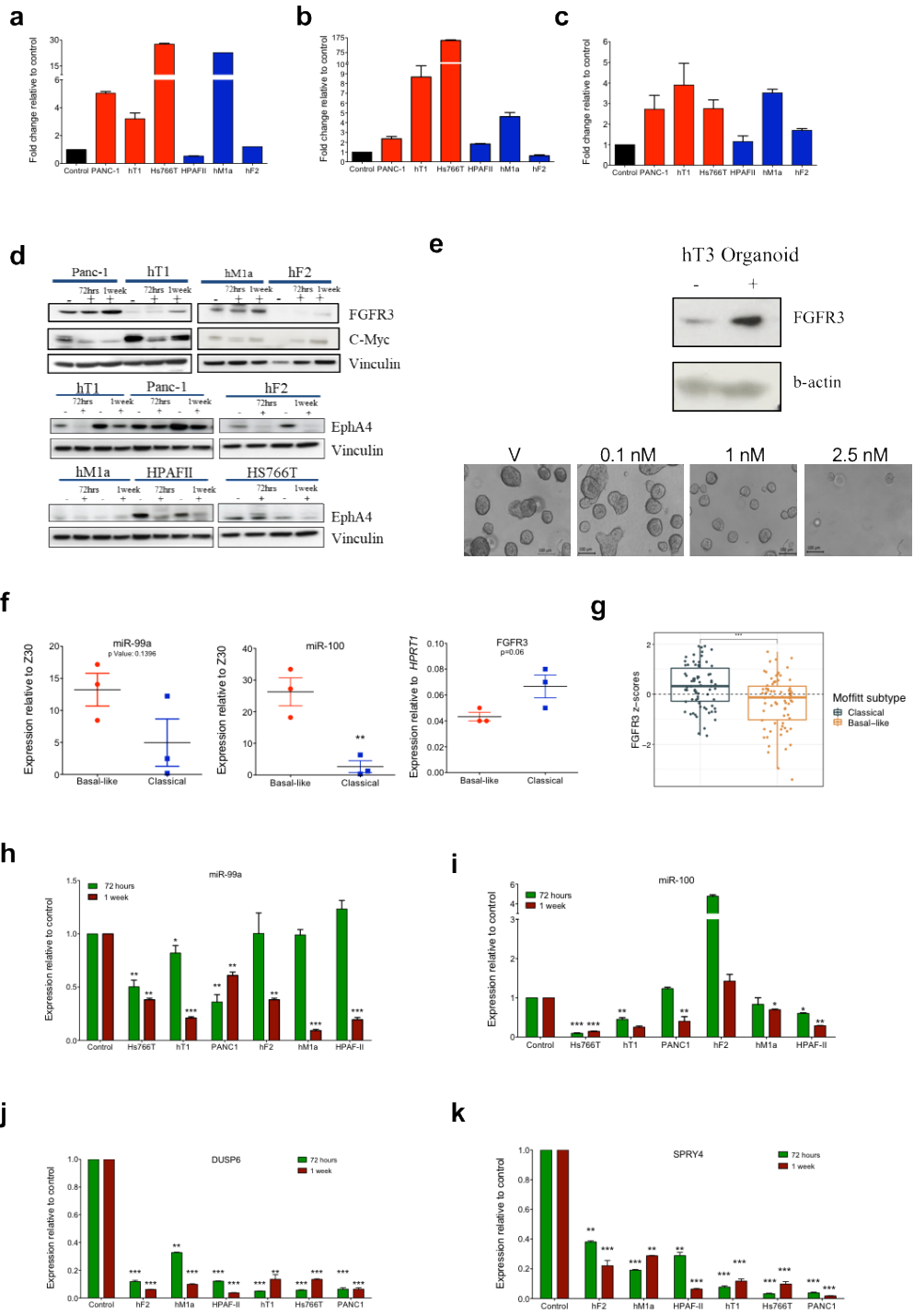


**Figure 4. Potential mechanisms of increased FGFR3 expression in PDAC following MEK inhibition.** **a** Changes in mRNA levels of *FGFR3* in basal-like (n = 3, red) and classical (n = 3, blue) cell lines following two days of MEKi. **b** Changes in mRNA levels of *FGFR3* in basal-like (n = 3, red) and classical (n = 3, blue) cell lines following seven days of MEKi. **c** Changes in mRNA levels of *EPHA4* in basal-like (n = 3, red) and classical (n = 3, blue) cell lines following two days of MEKi. In a-c, levels of individual genes were normalized to *HPRT1*, and then levels of the gene following treatment were normalized to those of the vehicle control. Data are displayed as average of three independent experiments with SEM. **d** Immunoblot analysis of selected effectors of FGFR3, EPHA4, and MYC in PDAC cell lines following 72 hours and 1 week of MEKi treatment. Vinculin was used as loading control. **e** A patient derived organoid culture (hT3) was treated continuously with different doses of MEKi, for ten days and effects on organoid size/numbers were evaluated at microscope. The right panel reports the immunoblot analysis for FGFR3 in hT3 following 24 hours of MEKi treatment. Beta-actin was used as loading control. **f** Expression of miR-99a (left panel), miR-100 (middle panel) and *FGFR3* (right panel) in PDAC cell lines defined either as basal-like (n = 3, red) or classical (n = 3, blue). Levels of microRNAs in individual cell lines were normalized to those of the housekeeping Z30. Data are displayed as scatter dot plots error bars indicating standard error of the means (SEM). P values were calculated by Student's t test. \*\*, p<0.01. **g** FGFR3 z-score stratified by Moffit subtypes in the TCGA PDAC cohort. \*\*\*, p<0.001 as determined by Wilcoxon rank-sum test. **h** Changes in the levels of miR-99a in individual PDAC cell lines following 72 hours and one week of MEKi. **i** Changes in the levels of miR-100 in individual PDAC cell lines following 72 hours and one week of MEKi. **j** Changes in mRNA levels of *DUSP6* in individual PDAC cell lines following 72 hours and one week of MEKi. **k** Changes in mRNA levels of *SPRY4* in individual PDAC cell lines following 72 hours and one

week of MEKi. In h-k, levels of individual genes were normalized to housekeeping, and then levels of the gene following treatment were normalized to those of the vehicle control. Data are displayed as average of three independent experiments with SEM. Statistical associations by Students' t test. \*\*\*,  $p < 0.001$ ; \*\*,  $p < 0.01$ ; \*,  $p < 0.05$ .

## **Connectivity Map analysis nominated HDAC and FGFR inhibitor as candidate for combinatorial treatment with MEKi**

Signalling pathways affect cellular processes through direct influence on the transcription of specific genes <sup>49</sup>. Drug-induced transcriptional changes may expose processes involved in cellular adaptation to the specific treatment, and therefore nominate candidate pathways/processes to be targeted in order to enhance treatment efficacy. Therefore, we probed MEKi induced transcriptional changes (**Supplementary Table 2**) against mRNA signatures arising from genetic and pharmacological perturbation of cell lines bearing genetic activation of MAP Kinase (*KRAS* or *BRAF* mutations) in the Connectivity Map (CMAP) database <sup>32</sup>. CMAP uses a pattern-matching algorithm, therefore perturbations that lead to highly similar, or highly dissimilar, mRNA signatures are termed “connected”. Positively correlated signatures might suggest that a given perturbation has similar physiological effects on the cells, while negatively correlated signatures might suggest that a given perturbation has opposing effects on the cells, thereby representing a potential candidate for therapeutic purposes. As expected, the perturbation class “MEK inhibitor” was found to produce mRNA changes highly-correlated to trametinib-induced transcriptional changes in our cell lines (Figures **5a-c**). Interestingly, another perturbation class highly correlated to our RNA signatures consisted of loss of function (LOF) of Lysine Acetyltransferases (Figures 5a-b). This perturbation class includes enzymes that are involved in acetylation of histones at lysine residues, known epigenetic marks that are usually associated to increased transcription. Intuitively, loss of acetyltransferase activity would reduce histones’ acetylation levels and produce a phenotype that could be counteracted by inhibition of enzymes involved in histone

deacetylation (histone deacetylases, HDAC). Therefore, we reasoned that histone deacetylases inhibitors (HDACi) could be a candidate compound class to elicit opposing, and therefore therapeutically meaningful, effects to MEKi. In line with our previous observation on the activation of FGFR3 signalling, the perturbation class “FGFR inhibitor” was found to elicit mRNA changes negatively correlated to trametinib-induced transcriptional changes in our cell lines (Figures 5a-d). In conclusion, CMAP analysis nominated FGFRi and HDCAi as potential drug classes that might synergize with MEKi for the treatment of PDAC. We tested this hypothesis by treated PDAC cell lines with combination of MEKi with either the HDAC inhibitor vorinostat and the FGFR inhibitor dovitinib. As expected we found that both HDACi and FGFRi sensitized PDAC cells to MEKi (Figures 5e-f).

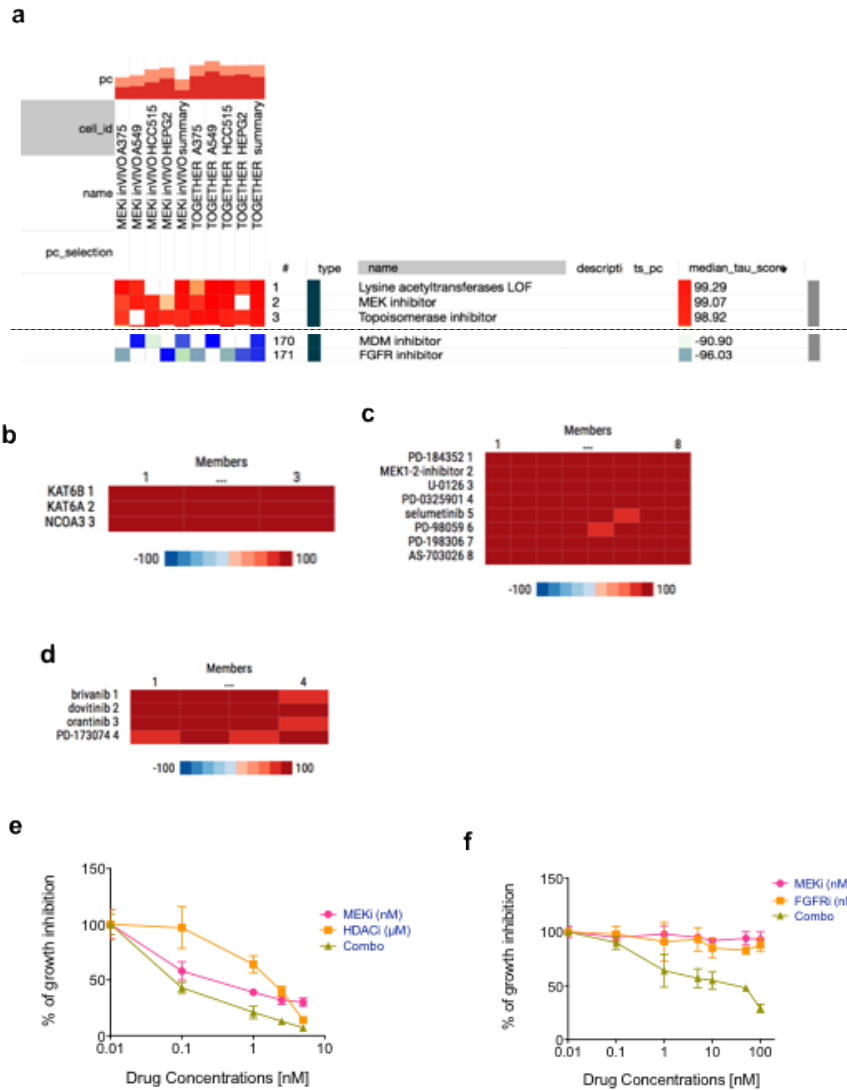


**Figure 5. Connectivity MAP analyses nominated candidates for combinatorial treatment.** **a** MEK inhibition is highly associated with external signatures of “Lysine acetyltransferases LOF” (loss of function), “MEK inhibitor”, and “Topoisomerase inhibitor”. MEK inhibition is inversely correlated to external signature of “FGFR inhibitor”. Data are displayed as a “barview” composed of horizontal lines, each representing a perturbation class instance, ordered by their corresponding connectivity score (median\_tau\_score). Red colour indicates highly associated signatures, blue colour indicates inversely correlated signatures. The type of instance (dark blue, perturbation class), the rank, the name of the perturbation class [name]

are provided. Images were modified to include only highly associated signatures. **b-d** Heatmap of the connectivity between members of the classes, across cell lines, where dark red represents the highest positive scores and deep blue the highest negative scores. Members of the class are displayed on the left. Heatmap in (b) refers to Lysine acetyltransferases LOF; heatmap in (c) refers to MEK inhibitor; and heatmap in (d) refers to FGFR inhibitor. **e** Dose-response curves of 5114 3D cell line treated with MEKi (Trametinib), HDACi (vorinostat) and MEKi + HDACi (Combo). **f** Dose-response curves of PANC-1 cell line treated with MEKi (Trametinib), FGFRi (dovitinib) and MEKi + FGFRi (Combo). For all curves, error bars represent standard deviation. When combinations of drugs were used, the EC50 of each drug was determined and the ratio the two EC50 calculated. Dose ranges of each drug were then calculated, keeping this EC50 ratio constant. For MEKi + HDACi the ratio is 1:1000, while for MEKi + FGFRi the calculated ratio was 1:10.

## CONCLUSIONS

In this study, we investigated the molecular determinants of resistance to an allosteric inhibitor of MEK1/2 (Trametinib) in PDAC. We demonstrated that effective inhibition of MEK1/2 elicits transcriptional upregulation and activation of FGFR3, and that combination of MEK and FGFR inhibitors is effective in reducing PDAC cells viability *in vitro*.

In this study, we deployed different models of the disease ranging from cell cultures to mouse tumour isografts, which strengthen the validity of our findings.

Although different studies have explored adaptive bypass mechanisms to MEK inhibition<sup>50,51</sup>, this is the first study to provide an integrative approach that rigorously combines proteomic and transcriptomic analyses to nominate a candidate mechanism of resistance to target therapy in PDAC.

Unfortunately, specific FGFR3 inhibitors that spare other members of the FGFRs family are not available, which warrants development of novel compounds in order to avoid excessive toxicities due to unwanted targeting.

We found that human PDAC cell lines display differential sensitivity to the inhibition of MEK, with squamous/basal-like cells being insensitive to both to short- and long-term treatments. When using suboptimal doses of MEKi, almost all PDAC cells demonstrated rewiring of the index oncogenic signalling at one week of continuous treatment. This suggested the engagement of adaptive bypass mechanisms to reactivate the drug-targeted pathway, which often encompasses increased expression and activation of Receptor Tyrosine Kinases. Increased signalling through RTKs can result from augmented expression of the receptor(s), increased level of

ligands, or downregulation of negative regulators of the pathway. This compensatory phenomenon is well known and has been described previously as mechanism of resistance to MEK inhibition in Kras-mutants non-small cell lung cancer<sup>36</sup>.

Therefore, we leveraged a mismatching time points RNA-seq experiment to exclude stress-related transcriptional responses and to identify changes in the kinome with direct functional relevance to the specific perturbation. Combining RNAseq data with a phospho-proteomic analysis of 49 RTKs, we identified activation of FGFR3 as potential mechanism of resistance to MEK inhibition. Increased phosphorylation of FGFR3 and its downstream effector FRS2 was observed in almost all cell lines analysed, thereby suggesting a common biochemical response to MEK inhibition in PDAC regardless of the molecular subtype.

We also demonstrated that increased expression and activation of FGFR3 in MEKi-treated PDAC cells was associated to reduced expression of 2 microRNAs (miR-99a and miR-100), which are known to regulate FGFR3 expression, as well as reduced levels of two negative regulators of the pathway (DUSP6 and SPRY4).

Drug-induced transcriptional changes may expose processes involved in cellular adaptation to the specific treatment, and therefore nominate candidate pathways/processes to be targeted to enhance treatment efficacy. Therefore, we probed MEKi induced transcriptional changes against mRNA signatures arising from genetic and pharmacological perturbation of cell lines bearing genetic activation of MAP Kinase (*KRAS* or *BRAF* mutations) in the Connectivity Map (CMAP) database<sup>32</sup>. CMAP uses a pattern-matching algorithm, therefore

perturbations that lead to highly similar, or highly dissimilar, mRNA signatures are termed “connected”. FGFR signalling was also nominated as candidate oncogenic signalling pathway for combinatorial treatment by interrogation of the CMAP database. Consistently, we demonstrated that FGFR inhibition sensitizes PDAC cells to MEK inhibition *in vitro*. Testing of the combination in an *in vivo* model of the disease will be necessary for a thorough preclinical validation of the proposed combination.

## BIBLIOGRAPHY

- 1 Who. Cancer. *World Health Organization* (2018).
- 2 Matsubayashi, H. *et al.* Familial pancreatic cancer: Concept, management and issues. *World J Gastroenterol* **23**, 935-948, doi:10.3748/wjg.v23.i6.935 (2017).
- 3 Spadi, R. *et al.* Current therapeutic strategies for advanced pancreatic cancer: A review for clinicians. *World Journal of Clinical Oncology* **7**, 27-43, doi:10.5306/wjco.v7.i1.27 (2016).
- 4 Cancer Genome Atlas, N. Comprehensive molecular portraits of human breast tumours. *Nature* **490**, 61-70, doi:10.1038/nature11412 (2012).
- 5 Cancer Genome Atlas Research, N. The Molecular Taxonomy of Primary Prostate Cancer. *Cell* **163**, 1011-1025, doi:10.1016/j.cell.2015.10.025 (2015).
- 6 Guinney, J. *et al.* The consensus molecular subtypes of colorectal cancer. *Nature Medicine* **21**, 1350-1356, doi:10.1038/nm.3967 (2015).
- 7 Distler, M., Aust, D., Weitz, J., Pilarsky, C. & Grützmann, R. Precursor lesions for sporadic pancreatic cancer: PanIN, IPMN, and MCN. *BioMed Research International* **2014**, 474905, doi:10.1155/2014/474905 (2014).
- 8 Hilgers, W., Rosty, C. & Hahn, S. A. Molecular pathogenesis of pancreatic cancer. *Hematology/Oncology Clinics of North America* **16**, 17-35, v (2002).
- 9 Lariño Noia, J. [Latest advances in pancreatic tumors]. *Gastroenterologia Y Hepatologia* **36 Suppl 2**, 90-97, doi:10.1016/S0210-5705(13)70059-1 (2013).
- 10 Distler, M., Aust, D., Weitz, J., Pilarsky, C. & Grutzmann, R. Precursor lesions for sporadic pancreatic cancer: PanIN, IPMN, and MCN. *Biomed Res Int* **2014**, 474905, doi:10.1155/2014/474905 (2014).
- 11 Society, A. C. Cancer Facts & Figures 2007. *American Cancer Society* (2007).
- 12 gene mutations
- 13 Makohon-Moore, A. & Iacobuzio-Donahue, C. A. Pancreatic cancer biology and genetics from an evolutionary perspective. *Nat Rev Cancer* **16**, 553-565, doi:10.1038/nrc.2016.66 (2016).
- 14 Haoqiang ying
- 15 Waddell, N. *et al.* Whole genomes redefine the mutational landscape of pancreatic cancer. *Nature* **518**, 495-501, doi:10.1038/nature14169 (2015).
- 16 Raphael, B. J. *et al.* Integrated Genomic Characterization of Pancreatic Ductal Adenocarcinoma. *Cancer Cell* **32**, 185-203.e113, doi:10.1016/j.ccell.2017.07.007 (2017).

- 17 Collisson, E. A. *et al.* Subtypes of pancreatic ductal adenocarcinoma and their differing responses to therapy. *Nat Med* **17**, 500-503, doi:10.1038/nm.2344 (2011).
- 18 Bailey, P. *et al.* Genomic analyses identify molecular subtypes of pancreatic cancer. *Nature* **531**, 47-52, doi:10.1038/nature16965 (2016).
- 19 Du, Y. *et al.* Molecular Subtyping of Pancreatic Cancer: Translating Genomics and Transcriptomics into the Clinic. *Journal of Cancer* **8**, 513-522, doi:10.7150/jca.17622 (2017).
- 20 Moffitt, R. A. *et al.* Virtual microdissection identifies distinct tumor- and stroma-specific subtypes of pancreatic ductal adenocarcinoma. *Nature genetics* **47**, 1168-1178, doi:10.1038/ng.3398 (2015).
- 21 Collisson, E. A. *et al.* Subtypes of Pancreatic Ductal Adenocarcinoma and Their Differing Responses to Therapy. *Nature medicine* **17**, 500-503, doi:10.1038/nm.2344 (2011).
- 22 Garnett, M. J. *et al.* Systematic identification of genomic markers of drug sensitivity in cancer cells. *Nature* **483**, 570-575, doi:10.1038/nature11005 (2012).
- 23 Falasca, M., Kim, M. & Casari, I. Pancreatic cancer: Current research and future directions. *Biochimica Et Biophysica Acta* **1865**, 123-132, doi:10.1016/j.bbcan.2016.01.001 (2016).
- 24 Torres, C. & Grippo, P. J. Pancreatic cancer subtypes: a roadmap for precision medicine. *Annals of Medicine* **50**, 277-287, doi:10.1080/07853890.2018.1453168 (2018).
- 25 Cox, A. D., Fesik, S. W., Kimmelman, A. C., Luo, J. & Der, C. J. Drugging the undruggable RAS: Mission possible? *Nat Rev Drug Discov* **13**, 828-851, doi:10.1038/nrd4389 (2014).
- 26 Waters, A. M. & Der, C. J. KRAS: The Critical Driver and Therapeutic Target for Pancreatic Cancer. *Cold Spring Harbor Perspectives in Medicine* **8**, a031435, doi:10.1101/cshperspect.a031435 (2018).
- 27 Bryant, K. L., Mancias, J. D., Kimmelman, A. C. & Der, C. J. KRAS: feeding pancreatic cancer proliferation. *Trends in Biochemical Sciences* **39**, 91-100, doi:10.1016/j.tibs.2013.12.004 (2014).
- 28 Boj, S. F. *et al.* Organoid models of human and mouse ductal pancreatic cancer. *Cell* **160**, 324-338, doi:10.1016/j.cell.2014.12.021 (2015).
- 29 Dobin, A. *et al.* STAR: ultrafast universal RNA-seq aligner. *Bioinformatics* **29**, 15-21, doi:10.1093/bioinformatics/bts635 (2013).
- 30 Love, M. I., Huber, W. & Anders, S. Moderated estimation of fold change and dispersion for RNA-seq data with DESeq2. *Genome Biol* **15**, 550, doi:10.1186/s13059-014-0550-8 (2014).

- 31 Max, R. & Hannah, R. Our World in Data. *Our World in Data* (2015).
- 32 Lamb, J. *et al.* The Connectivity Map: using gene-expression signatures to connect small molecules, genes, and disease. *Science* **313**, 1929-1935, doi:10.1126/science.1132939 (2006).
- 33 Cancer Genome Atlas Research Network. Electronic address, a. a. d. h. e. & Cancer Genome Atlas Research, N. Integrated Genomic Characterization of Pancreatic Ductal Adenocarcinoma. *Cancer Cell* **32**, 185-203 e113, doi:10.1016/j.ccell.2017.07.007 (2017).
- 34 Aung, K. L. *et al.* Genomics-Driven Precision Medicine for Advanced Pancreatic Cancer: Early Results from the COMPASS Trial. *Clin Cancer Res* **24**, 1344-1354, doi:10.1158/1078-0432.CCR-17-2994 (2018).
- 35 Moffitt, R. A. *et al.* Virtual microdissection identifies distinct tumor- and stroma-specific subtypes of pancreatic ductal adenocarcinoma. *Nat Genet* **47**, 1168-1178, doi:10.1038/ng.3398 (2015).
- 36 Konieczkowski, D. J., Johannessen, C. M. & Garraway, L. A. A Convergence-Based Framework for Cancer Drug Resistance. *Cancer Cell* **33**, 801-815, doi:10.1016/j.ccell.2018.03.025 (2018).
- 37 Kawai, T. *et al.* Interferon-alpha induction through Toll-like receptors involves a direct interaction of IRF7 with MyD88 and TRAF6. *Nat Immunol* **5**, 1061-1068, doi:10.1038/ni1118 (2004).
- 38 Davies, K. D. & Doebele, R. C. Molecular pathways: ROS1 fusion proteins in cancer. *Clin Cancer Res* **19**, 4040-4045, doi:10.1158/1078-0432.CCR-12-2851 (2013).
- 39 Turner, N. & Grose, R. Fibroblast growth factor signalling: from development to cancer. *Nat Rev Cancer* **10**, 116-129, doi:10.1038/nrc2780 (2010).
- 40 Malchers, F. *et al.* Cell-autonomous and non-cell-autonomous mechanisms of transformation by amplified FGFR1 in lung cancer. *Cancer Discov* **4**, 246-257, doi:10.1158/2159-8290.CD-13-0323 (2014).
- 41 Frattini, V. *et al.* A metabolic function of FGFR3-TACC3 gene fusions in cancer. *Nature* **553**, 222-227, doi:10.1038/nature25171 (2018).
- 42 Yokote, H. *et al.* Trans-activation of EphA4 and FGF receptors mediated by direct interactions between their cytoplasmic domains. *Proc Natl Acad Sci U S A* **102**, 18866-18871, doi:10.1073/pnas.0509741102 (2005).
- 43 Ruess, D. A. *et al.* Mutant KRAS-driven cancers depend on PTPN11/SHP2 phosphatase. *Nat Med* **24**, 954-960, doi:10.1038/s41591-018-0024-8 (2018).

- 44 Blick, C. *et al.* Hypoxia regulates FGFR3 expression via HIF-1alpha and miR-100 and contributes to cell survival in non-muscle invasive bladder cancer. *Br J Cancer* **109**, 50-59, doi:10.1038/bjc.2013.240 (2013).
- 45 Parker, B. C. *et al.* The tumorigenic FGFR3-TACC3 gene fusion escapes miR-99a regulation in glioblastoma. *J Clin Invest* **123**, 855-865, doi:10.1172/JCI67144 (2013).
- 46 Pratilas, C. A. & Solit, D. B. Targeting the mitogen-activated protein kinase pathway: physiological feedback and drug response. *Clin Cancer Res* **16**, 3329-3334, doi:10.1158/1078-0432.CCR-09-3064 (2010).
- 47 Sasaki, A., Taketomi, T., Wakioka, T., Kato, R. & Yoshimura, A. Identification of a dominant negative mutant of Sprouty that potentiates fibroblast growth factor- but not epidermal growth factor-induced ERK activation. *J Biol Chem* **276**, 36804-36808, doi:10.1074/jbc.C100386200 (2001).
- 48 Hanafusa, H., Torii, S., Yasunaga, T. & Nishida, E. Sprouty1 and Sprouty2 provide a control mechanism for the Ras/MAPK signalling pathway. *Nat Cell Biol* **4**, 850-858, doi:10.1038/ncb867 (2002).
- 49 Hanahan, D. & Weinberg, R. A. The hallmarks of cancer. *Cell* **100**, 57-70 (2000).
- 50 Mirzoeva, O. K. *et al.* Subtype-Specific MEK-PI3 Kinase Feedback as a Therapeutic Target in Pancreatic Adenocarcinoma. *Molecular Cancer Therapeutics* **12**, 2213-2225, doi:10.1158/1535-7163.MCT-13-0104 (2013).
- 51 Manchado, E. *et al.* A combinatorial strategy for treating KRAS-mutant lung cancer. *Nature* **534**, 647-651, doi:10.1038/nature18600 (2016).

## **APPENDIX**

**Figure S1.** MEKi induces kinome reprogramming in vivo.

**Figure S2.** Phospho-RTK analysis of PDAC cell lines treated with MEKi

**Supplementary Table 1.** Tyrosine Kinase genes deregulated following MEKi in human PDAC (related to Figure 3b)

**Supplementary Table 2.** List of 300 deregulated genes used for CMAP analysis (related to Figure 5)

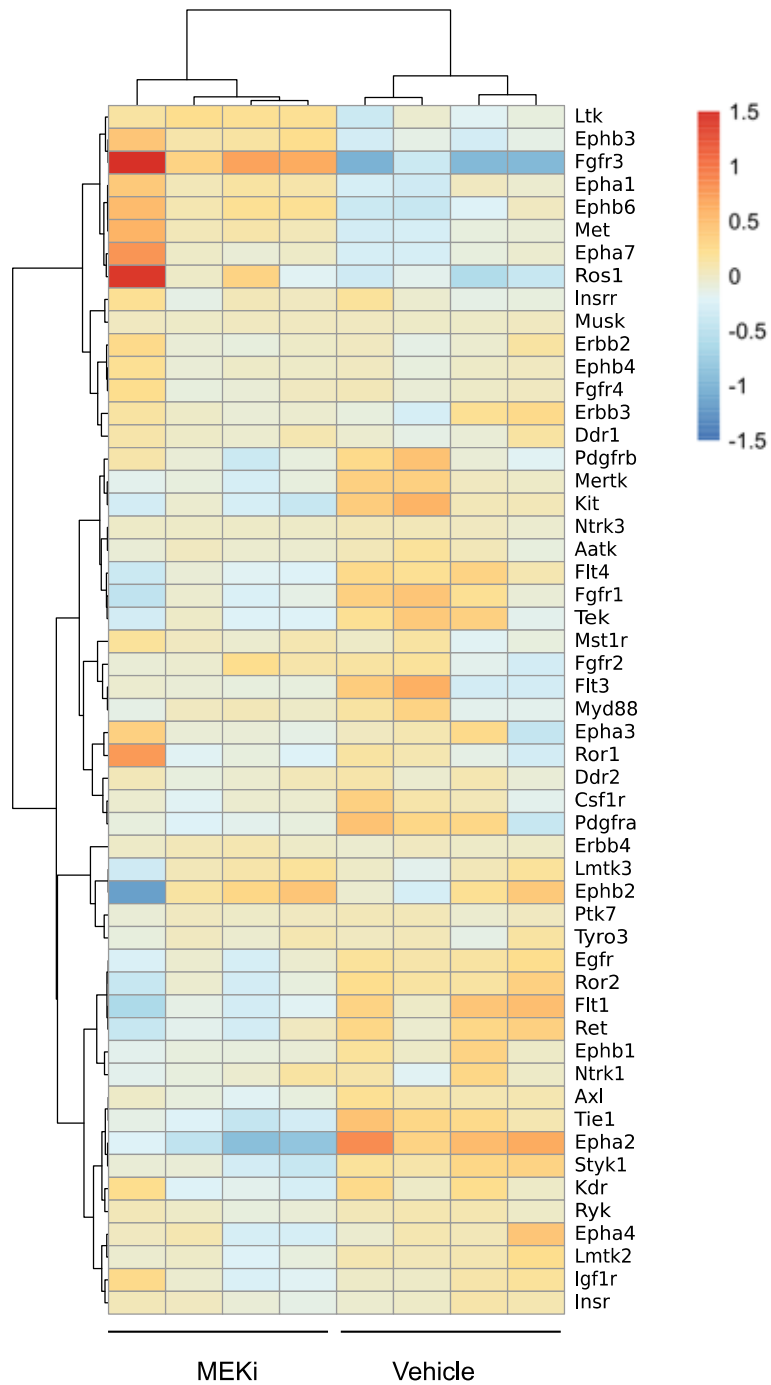
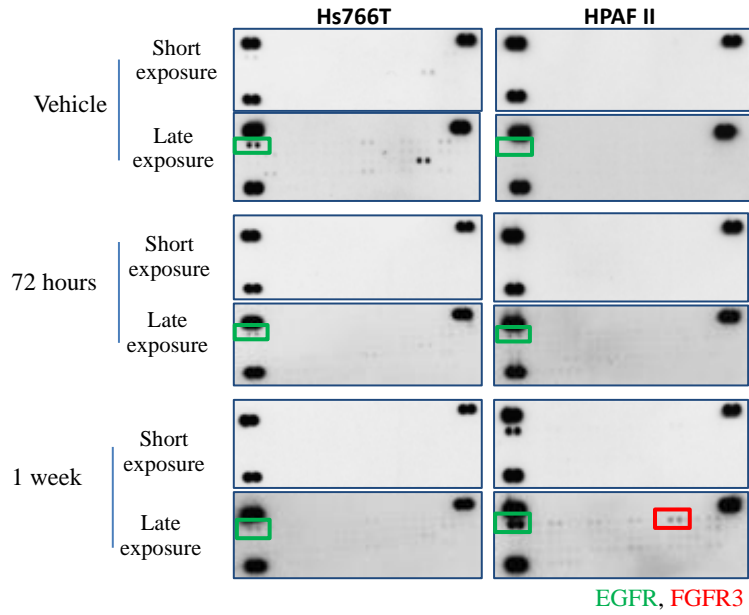


**Figure S1. MEKi induces kinome reprogramming in vivo.** DESeq2 analysis comparing MEKi with vehicle control. Shown are differentially expressed RTK genes (log<sub>2</sub> fold change). Mouse isografts were established

using mouse PDAC cell lines transplanted orthotopically into syngeneic mice. Tumor-bearing mice were treated either with vehicle (n =4) or MEKi (1mg/kg daily, n = 4) for 7 consecutive days before sacrifice.

**a**



**b**

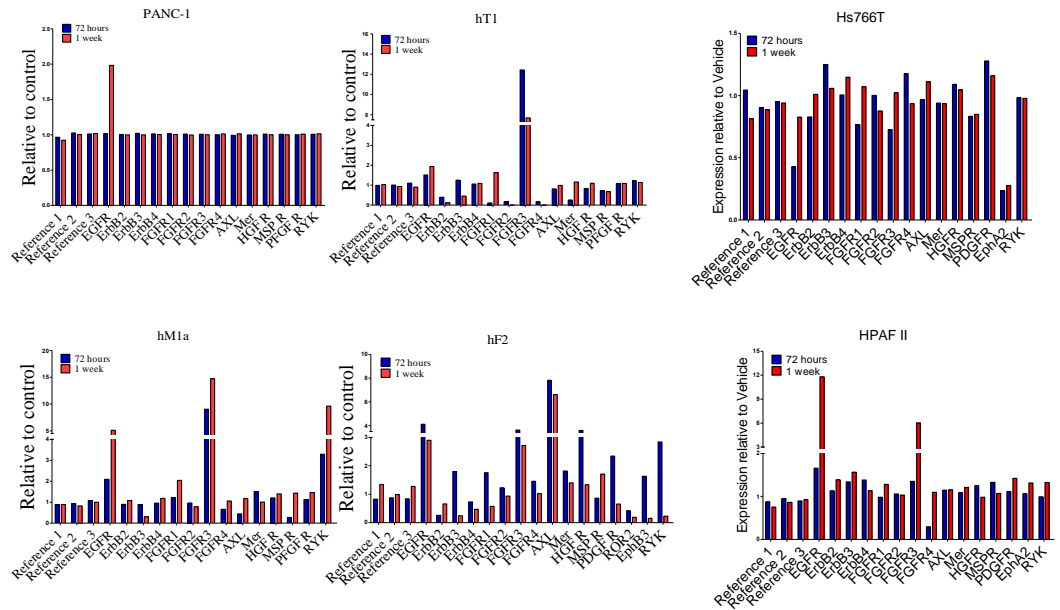


**Figure S2. Phospho-RTK analysis of PDAC cell lines treated with MEKi.**

**a** Phospho-RTKs arrays of Hs766t and HPAF-II treated with MEKi for 72 hours and 1 week. Signals referring to phospho-EGFR and phospho-FGFR3 are indicated by green and red circles, respectively. Both short and late

exposures are provided. **b** Quantification of changes in phospho-RTKs after treatment with MEKi for 72 hours and 1 week relative to DMSO. Values less than 0 indicate non-detectable RTKs

Supplementary Table 1. Tyrosine Kinase genes deregulated following MEKi in human PDAC (related to Figure 3b)

| ensembl_gene_id | baseMean    | log2FoldChange | lfcSE       | stat         | pvalue     | padj        | hgnc_symbol | gene_biotype   |
|-----------------|-------------|----------------|-------------|--------------|------------|-------------|-------------|----------------|
| ENSG00000172936 | 3773.72223  | 0.808902291    | 0.250368405 | 3.230848114  | 0.00123424 | 0.125995625 | MYD88       | protein_coding |
| ENSG00000608078 | 896.4654709 | 2.451651911    | 0.818244777 | 2.996232887  | 0.00273338 | 0.177692698 | FGFR3       | protein_coding |
| ENSG00000047936 | 54.24832616 | 4.347737343    | 1.704817797 | 2.550265108  | 0.0107641  | 0.296724321 | ROS1        | protein_coding |
| ENSG00000105397 | 1766.919111 | 0.25813004     | 0.113227557 | 2.279745725  | 0.02262277 | 0.386820457 | TYK2        | protein_coding |
| ENSG00000162434 | 7998.064568 | 0.518622986    | 0.296575332 | 1.748705743  | 0.0803419  | 0.59618851  | JAK1        | protein_coding |
| ENSG00000181409 | 275.4352295 | 1.725852833    | 0.995945016 | 1.732879632  | 0.08311707 | 0.601001744 | AATK        | protein_coding |
| ENSG00000141736 | 6068.322179 | 0.708739223    | 0.422794884 | 1.676319298  | 0.09367567 | 0.628959861 | ERBB2       | protein_coding |
| ENSG00000174292 | 382.6601268 | 0.685999195    | 0.42329241  | 1.620627204  | 0.10509761 | 0.65161374  | TNK1        | protein_coding |
| ENSG00000254087 | 1290.65493  | 0.407204146    | 0.254379132 | 1.600776533  | 0.10942642 | 0.661800263 | LYN         | protein_coding |
| ENSG00000204580 | 9567.527379 | 0.552716566    | 0.359944783 | 1.535559317  | 0.1246465  | 0.684793053 | DDR1        | protein_coding |
| ENSG00000142627 | 7902.838781 | -0.633552884   | 0.428578542 | -1.478265525 | 0.13933672 | 0.700443268 | EPHA2       | protein_coding |
| ENSG00000140443 | 1684.459915 | 0.361684869    | 0.260234561 | 1.389841793  | 0.16457692 | 0.730518151 | IGF1R       | protein_coding |
| ENSG00000125508 | 38.56307005 | 0.822231387    | 0.599758024 | 1.370938534  | 0.17039412 | 0.739940573 | SRMS        | protein_coding |
| ENSG00000164078 | 2646.312188 | -0.430056011   | 0.317871504 | -1.352924076 | 0.17607989 | 0.750131744 | MST1R       | protein_coding |
| ENSG00000120899 | 1193.557796 | 0.681133731    | 0.509535796 | 1.336773073  | 0.18129672 | 0.758981938 | PTK2B       | protein_coding |
| ENSG00000178568 | 12.97698461 | 1.053475956    | 0.808000119 | 1.303806684  | 0.1922995  | 0.769402801 | ERBB4       | protein_coding |
| ENSG00000106123 | 913.2735064 | -1.374305013   | 1.065166547 | -1.290225475 | 0.19697238 | 0.771659431 | EPHB6       | protein_coding |
| ENSG00000171105 | 780.1345791 | 0.315493689    | 0.245661014 | 1.284264377  | 0.19904947 | 0.774505406 | INSR        | protein_coding |
| ENSG00000113721 | 23.41897305 | 1.337271251    | 1.092698353 | 1.223824716  | 0.22101836 | 0.79728475  | PDGFRB      | protein_coding |
| ENSG00000169398 | 6586.980337 | -0.280653819   | 0.237035444 | -1.184016258 | 0.23640663 | 0.811451739 | PTK2        | protein_coding |
| ENSG00000097007 | 2156.895939 | 0.342576514    | 0.290270824 | 1.180196166  | 0.2379222  | 0.812479391 | ABL1        | protein_coding |
| ENSG00000007264 | 4.592788358 | 1.055815268    | 0.94762118  | 1.114174409  | 0.26520437 | 0.835434754 | MATK        | protein_coding |
| ENSG00000044524 | 310.45385   | 1.364463986    | 1.260250121 | 1.082693001  | 0.27894471 | 0.844852966 | EPHA3       | protein_coding |
| ENSG00000171094 | 10.83227871 | 0.665745817    | 0.621111444 | 1.071862099  | 0.28378198 | 0.849290913 | ALK         | protein_coding |
| ENSG00000163785 | 3326.06515  | -0.102907518   | 0.096582329 | -1.065490126 | 0.28665419 | 0.851011033 | RYK         | protein_coding |
| ENSG00000101213 | 1056.57578  | 0.362495375    | 0.344615951 | 1.051882173  | 0.29285361 | 0.854893795 | PTK6        | protein_coding |
| ENSG00000153208 | 480.2462341 | -0.675071735   | 0.663994156 | -1.016683248 | 0.30930414 | 0.867039493 | MERTK       | protein_coding |
| ENSG00000037280 | 7.123792923 | 1.066118181    | 1.072261588 | 0.994270607  | 0.32009114 | 0.875429456 | FLT4        | protein_coding |
| ENSG0000011816  | 1255.589246 | 0.71929502     | 0.75149733  | 0.957149135  | 0.33849199 | 0.888787537 | FRK         | protein_coding |
| ENSG00000062524 | 13.62761624 | 0.776417976    | 0.844777942 | 0.919079366  | 0.35805406 | 0.901274587 | LTK         | protein_coding |
| ENSG00000061938 | 2119.851151 | 0.209714041    | 0.228957144 | 0.915953253  | 0.35969141 | 0.902034425 | TNK2        | protein_coding |
| ENSG00000074966 | 287.6087063 | -0.641167663   | 0.7150339   | -0.896695476 | 0.36988144 | 0.906719943 | TXK         | protein_coding |
| ENSG00000116106 | 1049.095206 | 0.918160957    | 1.033965148 | 0.88799991   | 0.3745408  | 0.907851963 | EPHA4       | protein_coding |
| ENSG00000142235 | 127.7018316 | 0.581029171    | 0.6707472   | 0.866241663  | 0.38635765 | 0.912415313 | LMTK3       | protein_coding |
| ENSG0000010810  | 681.8167835 | 0.734435345    | 0.853860916 | 0.860134632  | 0.38971483 | 0.913101299 | FYN         | protein_coding |
| ENSG00000151422 | 1305.316423 | 0.256967046    | 0.31778287  | 0.808624599  | 0.41873111 | 0.930633445 | FER         | protein_coding |
| ENSG00000182866 | 30.00747591 | -0.725859873   | 0.903795785 | -0.803123765 | 0.4219032  | 0.931891462 | LCK         | protein_coding |
| ENSG00000146648 | 9360.767818 | -0.240680258   | 0.314965625 | -0.764147701 | 0.44477923 | 0.940547834 | EGFR        | protein_coding |
| ENSG00000165731 | 41.27518476 | -0.780005886   | 1.02608766  | -0.760174707 | 0.44715016 | 0.940564457 | RET         | protein_coding |
| ENSG00000182578 | 27.03954564 | 0.626070821    | 0.916053448 | 0.683443551  | 0.49432661 | 0.958140669 | CSF1R       | protein_coding |
| ENSG00000060140 | 719.0004839 | -0.494794425   | 0.771134199 | -0.641645028 | 0.52110369 | 0.964653601 | STYK1       | protein_coding |
| ENSG00000105639 | 100.1821671 | 0.483981588    | 0.817279966 | 0.591859914  | 0.5539444  | 0.969259944 | JAK3        | protein_coding |
| ENSG00000164715 | 1719.069499 | 0.146236316    | 0.251867364 | 0.580608434  | 0.56150439 | 0.970462831 | LMTK2       | protein_coding |
| ENSG00000135605 | 214.4605291 | -0.218839303   | 0.382042933 | -0.572813378 | 0.56677106 | 0.971321018 | TEC         | protein_coding |
| ENSG00000077782 | 887.3992932 | -0.288584018   | 0.546583401 | -0.527978014 | 0.5975146  | 0.973895867 | FGFR1       | protein_coding |
| ENSG00000105976 | 12281.32566 | -0.224231351   | 0.445510785 | -0.503312959 | 0.61474426 | 0.978756001 | MET         | protein_coding |
| ENSG00000066468 | 101.8625798 | 0.553815618    | 1.118040444 | 0.495344887  | 0.62035669 | 0.979575966 | FGFR2       | protein_coding |
| ENSG00000182511 | 11.64045016 | 0.416228388    | 0.850430245 | 0.48943272   | 0.62453538 | 0.979961109 | FES         | protein_coding |
| ENSG00000160867 | 195.0361258 | 0.362187583    | 0.752106228 | 0.481564397  | 0.63011542 | 0.980547172 | FGFR4       | protein_coding |
| ENSG00000167601 | 7302.747057 | -0.359897881   | 0.751442693 | -0.478942552 | 0.6319795  | 0.980678926 | AXL         | protein_coding |
| ENSG00000157404 | 59.21716736 | 0.819932742    | 1.911903031 | 0.428856866  | 0.66802739 | 0.985271974 | KIT         | protein_coding |
| ENSG00000128052 | 45.4258645  | -0.785356082   | 1.931671977 | -0.406568036 | 0.68432528 | 0.987553988 | KDR         | protein_coding |
| ENSG00000162733 | 68.23618409 | 0.213001078    | 0.520716951 | 0.409053475  | 0.68250042 | 0.987553988 | DDR2        | protein_coding |
| ENSG00000182580 | 369.7102749 | 0.400525614    | 1.014666647 | 0.394736158  | 0.69303762 | 0.988487365 | EPHB2       | protein_coding |
| ENSG00000133216 | 1672.773553 | 0.204674964    | 0.602336248 | 0.339801838  | 0.73400576 | 0.990887184 | EPHB3       | protein_coding |
| ENSG00000092445 | 698.3484571 | -0.104273296   | 0.307506177 | -0.339093339 | 0.73453942 | 0.990887184 | TYRO3       | protein_coding |
| ENSG00000103653 | 1172.819738 | -0.095748452   | 0.272996893 | -0.350730923 | 0.72579022 | 0.990887184 | CSK         | protein_coding |
| ENSG00000143322 | 2367.648542 | 0.121947489    | 0.354265344 | 0.344226414  | 0.73067602 | 0.990887184 | ABL2        | protein_coding |
| ENSG00000102010 | 7.618923235 | -0.486327762   | 1.502903339 | -0.323592176 | 0.74624681 | 0.991929947 | BMX         | protein_coding |
| ENSG00000112655 | 2054.193643 | 0.353387124    | 1.136000672 | 0.311080031  | 0.75573978 | 0.992839448 | PTK7        | protein_coding |
| ENSG00000169071 | 38.79942389 | -0.38327691    | 1.323780542 | -0.289532062 | 0.77217425 | 0.995088859 | ROR2        | protein_coding |
| ENSG00000135333 | 37.8088153  | 0.555852886    | 1.988830436 | 0.279487319  | 0.77987087 | 0.995144016 | EPHA7       | protein_coding |
| ENSG00000120156 | 284.1321851 | -0.413636063   | 1.516580827 | -0.272742511 | 0.78505115 | 0.995154003 | TEK         | protein_coding |
| ENSG00000000938 | 11.51719594 | 0.415348945    | 1.577210488 | 0.263344016  | 0.79228544 | 0.995154003 | FGR         | protein_coding |
| ENSG00000146904 | 307.1650519 | 0.177584894    | 0.816317055 | 0.217544021  | 0.8277844  | 0.995781274 | EPHA1       | protein_coding |
| ENSG00000154928 | 30.32163417 | 0.175075409    | 0.697216027 | 0.251106403  | 0.80173185 | 0.995781274 | EPHB1       | protein_coding |
| ENSG00000196411 | 3225.456006 | 0.145891376    | 0.581772778 | 0.250770372  | 0.80199165 | 0.995781274 | EPHB4       | protein_coding |
| ENSG00000065361 | 4965.930266 | 0.165687644    | 0.804339311 | 0.205992225  | 0.83679699 | 0.995781274 | ERBB3       | protein_coding |
| ENSG00000197122 | 2341.188784 | 0.086907184    | 0.421702518 | 0.206086471  | 0.83672337 | 0.995781274 | SRC         | protein_coding |
| ENSG00000115085 | 4.061391204 | 0.197185738    | 0.954433114 | 0.206599849  | 0.83632238 | 0.995781274 | ZAP70       | protein_coding |
| ENSG00000165025 | 786.8078518 | -0.15197229    | 0.801298824 | -0.189657447 | 0.84957757 | 0.996468061 | SYK         | protein_coding |
| ENSG00000176105 | 3283.38142  | -0.057795735   | 0.337011005 | -0.171495098 | 0.86383448 | 0.997109231 | YES1        | protein_coding |
| ENSG00000096968 | 536.8825411 | -0.04504565    | 0.299932724 | -0.150185845 | 0.88061799 | 0.997370896 | JAK2        | protein_coding |
| ENSG00000145242 | 4.178577985 | 0.147456231    | 1.534047259 | 0.096122352  | 0.9234234  | 0.998824276 | EPHA5       | protein_coding |
| ENSG00000185483 | 879.9443391 | -0.093209371   | 0.762360813 | -0.122264116 | 0.90268985 | 0.998824276 | ROR1        | protein_coding |
| ENSG00000070886 | 0.650320403 | 1.314286124    | 1.78572027  | 0.735997763  | 0.46173206 | NA          | EPHA8       | protein_coding |
| ENSG00000102755 | 0.705975497 | 1.885528103    | 1.615265739 | 1.167317586  | 0.24308214 | NA          | FLT1        | protein_coding |
| ENSG00000122025 | 0.547175513 | -0.03389989    | 1.945470304 | -0.017425036 | 0.98609754 | NA          | FLT3        | protein_coding |
| ENSG00000027644 | 1.301457256 | 0.742827552    | 1.154109454 | 0.643637005  | 0.51981085 | NA          | INSRR       | protein_coding |
| ENSG00000101336 | 1.819005974 | -2.058336882   | 1.107095308 | -1.85922284  | 0.06299556 | NA          | MUSK        | protein_coding |
| ENSG00000198400 | 1.51280444  | 0.328008571    | 0.842521445 | 0.389317771  | 0.69704109 | NA          | NTRK1       | protein_coding |
| ENSG00000140538 | 0.272561963 | -1.547459897   | 2.912256281 | -0.531361167 | 0.59516853 | NA          | NTRK3       | protein_coding |
| ENSG00000134853 | 1.59763967  | -1.065039784   | 1.182547953 | -0.900631371 | 0.36778435 | NA          | PDGFRA      | protein_coding |
| ENSG00000066056 | 13.5029214  | -1.76199123    | 1.100561814 | -1.600992518 | NA         | NA          | TIE1        | protein_coding |
| ENSG00000101336 | 1.456932863 | 1.656355883    | 1.341009776 | 1.235155711  | 0.21677256 | NA          | HCK         | protein_coding |
| ENSG00000113263 | 3.000420223 | -0.929884621   | 1.543339733 | -0.602514535 | 0.54683169 | NA          | ITK         | protein_coding |
| ENSG00000136573 | 0.967982599 | 0.10377094     | 1.232838104 | 0.084172399  | 0.93291936 | NA          | BLK         | protein_coding |
| ENSG0000010671  | 1.601690681 | 0.030541504    | 1.126341458 | 0.02711567   | 0.97836748 | NA          | BTK         | protein_coding |

**Supplementary Table 2. List of 300 deregulated genes used for CMAP analysis.**

| hgnc_sym<br>bol | baseMean    | log2FoldC<br>hange | lfcSE  | stat     | pvalue   | padj     | direction |
|-----------------|-------------|--------------------|--------|----------|----------|----------|-----------|
| MYL7            | 32.44838518 | 4.516498           | 0.8428 | 5.358834 | 8.38E-08 | 8.19E-06 | UP        |
| OLR1            | 340.6205193 | 4.412644           | 0.4723 | 9.343133 | 9.35E-21 | 3.50E-17 | UP        |
| VTCN1           | 669.16924   | 4.344305           | 0.7736 | 5.615576 | 1.96E-08 | 2.65E-06 | UP        |
| APOBEC3A        | 53.57805789 | 4.16651            | 0.9101 | 4.578308 | 4.69E-06 | 1.94E-04 | UP        |
| C4orf54         | 23.98610479 | 3.882769           | 0.7684 | 5.052838 | 4.35E-07 | 3.18E-05 | UP        |
| ODAM            | 49.84265823 | 3.543412           | 0.7694 | 4.60524  | 4.12E-06 | 1.75E-04 | UP        |
| ROS1            | 54.24832616 | 3.512817           | 0.7722 | 4.549322 | 5.38E-06 | 2.14E-04 | UP        |
| KRT17           | 17704.33106 | 2.8761             | 0.4314 | 6.666327 | 2.62E-11 | 1.09E-08 | UP        |
| DRGX            | 21.58103294 | 2.612788           | 0.5496 | 4.754033 | 1.99E-06 | 1.05E-04 | UP        |
| UPK1A           | 114.8825229 | 2.54008            | 0.4779 | 5.31528  | 1.06E-07 | 9.96E-06 | UP        |
| CSDC2           | 54.2602604  | 2.478276           | 0.5104 | 4.855642 | 1.20E-06 | 7.04E-05 | UP        |
| GCNT4           | 406.6360261 | 2.469395           | 0.4434 | 5.568776 | 2.57E-08 | 3.17E-06 | UP        |
| SEMA5A          | 2271.606633 | 2.437556           | 0.3227 | 7.553242 | 4.25E-14 | 3.74E-11 | UP        |
| OPRD1           | 21.95546523 | 2.404992           | 0.5404 | 4.450755 | 8.56E-06 | 3.05E-04 | UP        |
| EDN2            | 404.8837099 | 2.374306           | 0.4280 | 5.547138 | 2.90E-08 | 3.53E-06 | UP        |
| MYL9            | 3705.049108 | 2.35064            | 0.4185 | 5.61719  | 1.94E-08 | 2.65E-06 | UP        |
| LUM             | 8174.504563 | 2.342767           | 0.4488 | 5.220595 | 1.78E-07 | 1.54E-05 | UP        |
| NEURL3          | 137.7336269 | 2.338681           | 0.4180 | 5.594965 | 2.21E-08 | 2.90E-06 | UP        |
| MRAS            | 660.0613806 | 2.337718           | 0.2897 | 8.068413 | 7.12E-16 | 9.69E-13 | UP        |
| RRAD            | 319.2000432 | 2.3259             | 0.4112 | 5.656416 | 1.55E-08 | 2.27E-06 | UP        |
| SERPING1        | 66.42361561 | 2.312898           | 0.4904 | 4.716064 | 2.40E-06 | 1.20E-04 | UP        |
| SAMD11          | 183.9426674 | 2.30888            | 0.4933 | 4.680786 | 2.86E-06 | 1.33E-04 | UP        |
| CFTR            | 28.64528478 | 2.274273           | 0.4200 | 5.414473 | 6.15E-08 | 6.45E-06 | UP        |
| DACT1           | 728.657433  | 2.273864           | 0.4768 | 4.769146 | 1.85E-06 | 9.91E-05 | UP        |
| GPR37L1         | 93.48359592 | 2.27332            | 0.3418 | 6.650073 | 2.93E-11 | 1.15E-08 | UP        |
| GPR1            | 402.1190491 | 2.272657           | 0.4243 | 5.35682  | 8.47E-08 | 8.23E-06 | UP        |
| WISP2           | 625.9051285 | 2.219765           | 0.3663 | 6.060087 | 1.36E-09 | 3.28E-07 | UP        |
| LTB             | 133.4552332 | 2.217657           | 0.4814 | 4.606479 | 4.10E-06 | 1.75E-04 | UP        |
| BMF             | 1292.788509 | 2.185834           | 0.3817 | 5.726424 | 1.03E-08 | 1.60E-06 | UP        |
| KRT16           | 1238.486029 | 2.184669           | 0.3097 | 7.054755 | 1.73E-12 | 1.04E-09 | UP        |
| TRIM29          | 5352.760573 | 2.178531           | 0.4037 | 5.395891 | 6.82E-08 | 6.94E-06 | UP        |
| SCN3B           | 21.91826855 | 2.130172           | 0.4746 | 4.488446 | 7.17E-06 | 2.70E-04 | UP        |
| C6orf222        | 51.42575452 | 2.123853           | 0.4177 | 5.085122 | 3.67E-07 | 2.75E-05 | UP        |
| DUSP8           | 163.7403115 | 2.123261           | 0.2912 | 7.290615 | 3.09E-13 | 2.10E-10 | UP        |
| IL32            | 2286.263956 | 2.120794           | 0.3351 | 6.329401 | 2.46E-10 | 7.52E-08 | UP        |
| CCDC80          | 8413.981328 | 2.108394           | 0.3738 | 5.640034 | 1.70E-08 | 2.42E-06 | UP        |
| KCNG1           | 56.25548182 | 2.105027           | 0.4195 | 5.017493 | 5.24E-07 | 3.61E-05 | UP        |
| NPY4R           | 60.45390926 | 2.090517           | 0.3887 | 5.378825 | 7.50E-08 | 7.48E-06 | UP        |
| GPRIN2          | 155.2179411 | 2.062664           | 0.3405 | 6.057474 | 1.38E-09 | 3.28E-07 | UP        |
| WNT10A          | 1059.071821 | 2.052214           | 0.4002 | 5.128013 | 2.93E-07 | 2.32E-05 | UP        |
| ACE2            | 153.6537025 | 2.037402           | 0.4098 | 4.971671 | 6.64E-07 | 4.35E-05 | UP        |
| PLA2G4C         | 215.9545971 | 2.022485           | 0.3298 | 6.133302 | 8.61E-10 | 2.22E-07 | UP        |
| TGM1            | 223.4671133 | 1.997386           | 0.3707 | 5.388503 | 7.10E-08 | 7.19E-06 | UP        |
| SPON2           | 448.1791966 | 1.987938           | 0.3979 | 4.995683 | 5.86E-07 | 3.97E-05 | UP        |
| TNNC1           | 408.8358467 | 1.951465           | 0.3604 | 5.414034 | 6.16E-08 | 6.45E-06 | UP        |
| SYNPO           | 8113.702086 | 1.940962           | 0.2298 | 8.445233 | 3.03E-17 | 4.54E-14 | UP        |
| ST6GALNAC       | 131.6393318 | 1.935654           | 0.3777 | 5.124665 | 2.98E-07 | 2.35E-05 | UP        |
| RASGEF1B        | 38.29258705 | 1.931065           | 0.3866 | 4.995582 | 5.87E-07 | 3.97E-05 | UP        |
| ID3             | 2498.439989 | 1.90974            | 0.3372 | 5.66368  | 1.48E-08 | 2.22E-06 | UP        |
| PLEKHG4B        | 217.0030007 | 1.884708           | 0.4058 | 4.64416  | 3.41E-06 | 1.53E-04 | UP        |
| COL12A1         | 6585.00206  | 1.860046           | 0.3515 | 5.291089 | 1.22E-07 | 1.12E-05 | UP        |
| MFAP3L          | 353.7330306 | 1.849788           | 0.3348 | 5.52579  | 3.28E-08 | 3.90E-06 | UP        |
| ADAMTSL4        | 390.4107843 | 1.844162           | 0.3034 | 6.077426 | 1.22E-09 | 3.00E-07 | UP        |
| C10orf67        | 100.0089864 | 1.839212           | 0.4166 | 4.415268 | 1.01E-05 | 3.45E-04 | UP        |
| FSTL3           | 4220.104934 | 1.820302           | 0.2357 | 7.724381 | 1.12E-14 | 1.29E-11 | UP        |
| ANXA8L1         | 3732.695084 | 1.810897           | 0.2501 | 7.241987 | 4.42E-13 | 2.76E-10 | UP        |
| LRRN1           | 3212.515839 | 1.799064           | 0.3763 | 4.781019 | 1.74E-06 | 9.46E-05 | UP        |
| PCDHB9          | 48.35152852 | 1.779522           | 0.3986 | 4.464016 | 8.04E-06 | 2.94E-04 | UP        |

|          |             |          |        |          |          |          |    |
|----------|-------------|----------|--------|----------|----------|----------|----|
| VASN     | 235.6463838 | 1.768033 | 0.2887 | 6.124587 | 9.09E-10 | 2.31E-07 | UP |
| CASZ1    | 306.2463482 | 1.753275 | 0.2421 | 7.242284 | 4.41E-13 | 2.76E-10 | UP |
| GPC1     | 8084.034253 | 1.713554 | 0.2226 | 7.698337 | 1.38E-14 | 1.47E-11 | UP |
| BAMBI    | 698.9677052 | 1.707296 | 0.3860 | 4.423085 | 9.73E-06 | 3.38E-04 | UP |
| IGFBP3   | 14285.61907 | 1.703673 | 0.3769 | 4.520117 | 6.18E-06 | 2.39E-04 | UP |
| AATK     | 275.4352295 | 1.695219 | 0.3684 | 4.601218 | 4.20E-06 | 1.77E-04 | UP |
| TLR5     | 61.14204065 | 1.663922 | 0.3478 | 4.784397 | 1.72E-06 | 9.34E-05 | UP |
| FOXO6    | 145.5306278 | 1.647812 | 0.3311 | 4.976651 | 6.47E-07 | 4.30E-05 | UP |
| MMP19    | 216.1999664 | 1.645674 | 0.3659 | 4.497277 | 6.88E-06 | 2.60E-04 | UP |
| MUC4     | 3619.867605 | 1.6186   | 0.3305 | 4.897268 | 9.72E-07 | 5.99E-05 | UP |
| CXCL16   | 1225.220951 | 1.608577 | 0.3235 | 4.972563 | 6.61E-07 | 4.35E-05 | UP |
| SLC7A7   | 1194.797192 | 1.598138 | 0.3035 | 5.265166 | 1.40E-07 | 1.26E-05 | UP |
| MYH14    | 4530.657672 | 1.594537 | 0.2619 | 6.089126 | 1.14E-09 | 2.83E-07 | UP |
| ABAT     | 411.542868  | 1.562838 | 0.2740 | 5.704081 | 1.17E-08 | 1.79E-06 | UP |
| TP53I11  | 1474.550574 | 1.547074 | 0.3262 | 4.742931 | 2.11E-06 | 1.08E-04 | UP |
| PIK3IP1  | 2483.307874 | 1.531034 | 0.3254 | 4.704816 | 2.54E-06 | 1.24E-04 | UP |
| HMOX1    | 1438.307558 | 1.500535 | 0.2616 | 5.735142 | 9.74E-09 | 1.57E-06 | UP |
| HSPB8    | 1011.289704 | 1.499113 | 0.2837 | 5.284459 | 1.26E-07 | 1.15E-05 | UP |
| NRG4     | 65.19510906 | 1.49021  | 0.3308 | 4.504639 | 6.65E-06 | 2.53E-04 | UP |
| NECTIN4  | 1178.389947 | 1.486082 | 0.2952 | 5.034281 | 4.80E-07 | 3.39E-05 | UP |
| BTG2     | 1043.563053 | 1.48477  | 0.2941 | 5.048488 | 4.45E-07 | 3.19E-05 | UP |
| ANXA8    | 10574.1152  | 1.46137  | 0.3147 | 4.643582 | 3.42E-06 | 1.53E-04 | UP |
| TMEM45A  | 458.3075939 | 1.451372 | 0.3163 | 4.588004 | 4.48E-06 | 1.86E-04 | UP |
| GAA      | 1304.712673 | 1.448616 | 0.2786 | 5.199171 | 2.00E-07 | 1.68E-05 | UP |
| TINCR    | 773.2612972 | 1.44192  | 0.2965 | 4.863013 | 1.16E-06 | 6.84E-05 | UP |
| DEPP1    | 815.4595564 | 1.437894 | 0.2906 | 4.947387 | 7.52E-07 | 4.87E-05 | UP |
| HLA-B    | 24859.33047 | 1.435958 | 0.2704 | 5.31036  | 1.09E-07 | 1.02E-05 | UP |
| CLIC3    | 510.4842448 | 1.434277 | 0.3038 | 4.721544 | 2.34E-06 | 1.18E-04 | UP |
| UPK2     | 1899.125089 | 1.423064 | 0.2223 | 6.402915 | 1.52E-10 | 5.07E-08 | UP |
| SLC22A23 | 169.6507141 | 1.419269 | 0.2854 | 4.97331  | 6.58E-07 | 4.35E-05 | UP |
| SECTM1   | 1055.167219 | 1.413856 | 0.2717 | 5.203244 | 1.96E-07 | 1.68E-05 | UP |
| STX11    | 53.1132039  | 1.405972 | 0.2948 | 4.768728 | 1.85E-06 | 9.91E-05 | UP |
| ABHD4    | 3696.541094 | 1.403984 | 0.2095 | 6.700098 | 2.08E-11 | 8.91E-09 | UP |
| METRNL   | 647.4143915 | 1.4022   | 0.2567 | 5.463414 | 4.67E-08 | 5.30E-06 | UP |
| SELENOM  | 723.2557838 | 1.401638 | 0.3014 | 4.649868 | 3.32E-06 | 1.49E-04 | UP |
| JAG2     | 1208.745404 | 1.390866 | 0.3136 | 4.434582 | 9.23E-06 | 3.24E-04 | UP |
| MYCL     | 417.6313206 | 1.379241 | 0.1567 | 8.801977 | 1.34E-18 | 3.35E-15 | UP |
| ULK1     | 1830.958078 | 1.376099 | 0.2394 | 5.747801 | 9.04E-09 | 1.49E-06 | UP |
| COL4A2   | 52.8118053  | 1.376019 | 0.2923 | 4.707094 | 2.51E-06 | 1.23E-04 | UP |
| DDIT4    | 676.7865038 | 1.351387 | 0.2932 | 4.609694 | 4.03E-06 | 1.73E-04 | UP |
| MB21D2   | 1121.506567 | 1.345951 | 0.2149 | 6.262781 | 3.78E-10 | 1.09E-07 | UP |
| CYP2J2   | 115.7141043 | 1.338162 | 0.2788 | 4.800247 | 1.58E-06 | 8.85E-05 | UP |
| TENT5B   | 274.8835354 | 1.337464 | 0.2706 | 4.942641 | 7.71E-07 | 4.95E-05 | UP |
| ARID5B   | 1321.117089 | 1.327014 | 0.2834 | 4.682757 | 2.83E-06 | 1.33E-04 | UP |
| CTSH     | 12958.51769 | 1.325389 | 0.2788 | 4.754665 | 1.99E-06 | 1.05E-04 | UP |
| TMPRSS3  | 543.6281694 | 1.322887 | 0.2874 | 4.603017 | 4.16E-06 | 1.76E-04 | UP |
| ATF3     | 747.5982235 | 1.31731  | 0.2950 | 4.466115 | 7.97E-06 | 2.92E-04 | UP |
| HSPB1    | 6828.623544 | 1.29839  | 0.2588 | 5.01635  | 5.27E-07 | 3.62E-05 | UP |
| SLC7A5   | 11850.1149  | 1.282624 | 0.2219 | 5.779587 | 7.49E-09 | 1.29E-06 | UP |
| RAG1     | 80.6352644  | 1.278982 | 0.2804 | 4.560561 | 5.10E-06 | 2.08E-04 | UP |
| HLA-C    | 20193.81538 | 1.277585 | 0.2350 | 5.436726 | 5.43E-08 | 5.84E-06 | UP |
| THBS1    | 28745.3215  | 1.260873 | 0.2774 | 4.544994 | 5.49E-06 | 2.17E-04 | UP |
| EPB41L4A | 502.6852891 | 1.255052 | 0.2487 | 5.04637  | 4.50E-07 | 3.19E-05 | UP |
| ELF3     | 6976.865815 | 1.245267 | 0.2818 | 4.418649 | 9.93E-06 | 3.42E-04 | UP |
| NUTM2D   | 68.83317249 | 1.240867 | 0.2583 | 4.803801 | 1.56E-06 | 8.73E-05 | UP |
| TRPM4    | 1060.84216  | 1.226988 | 0.2413 | 5.084086 | 3.69E-07 | 2.75E-05 | UP |
| FOSL2    | 6229.209334 | 1.208346 | 0.1577 | 7.660713 | 1.85E-14 | 1.85E-11 | UP |
| CTIF     | 1038.16556  | 1.205782 | 0.2503 | 4.817046 | 1.46E-06 | 8.29E-05 | UP |
| C1QTNF6  | 1628.749379 | 1.199703 | 0.1942 | 6.177199 | 6.52E-10 | 1.81E-07 | UP |
| TUFT1    | 4719.808391 | 1.171426 | 0.2009 | 5.831914 | 5.48E-09 | 1.01E-06 | UP |
| JUNB     | 1720.828687 | 1.17108  | 0.2220 | 5.274435 | 1.33E-07 | 1.20E-05 | UP |

|           |             |          |        |          |          |          |      |
|-----------|-------------|----------|--------|----------|----------|----------|------|
| SIK1B     | 340.8968116 | 1.169667 | 0.2105 | 5.556613 | 2.75E-08 | 3.37E-06 | UP   |
| LARGE1    | 252.9441319 | 1.168615 | 0.2371 | 4.929395 | 8.25E-07 | 5.19E-05 | UP   |
| CTSD      | 10460.75716 | 1.157075 | 0.2265 | 5.108853 | 3.24E-07 | 2.51E-05 | UP   |
| TLE4      | 661.3022363 | 1.150794 | 0.2574 | 4.471065 | 7.78E-06 | 2.88E-04 | UP   |
| DNAJB2    | 2973.567891 | 1.138644 | 0.1665 | 6.837243 | 8.07E-12 | 4.03E-09 | UP   |
| ATP2B4    | 8950.47327  | 1.138346 | 0.2313 | 4.921244 | 8.60E-07 | 5.34E-05 | UP   |
| CXXC5     | 2524.651891 | 1.136381 | 0.2517 | 4.514919 | 6.33E-06 | 2.44E-04 | UP   |
| CITED2    | 2540.023612 | 1.12835  | 0.1726 | 6.536926 | 6.28E-11 | 2.24E-08 | UP   |
| ATP6V1FNE | 103.5876551 | 1.09904  | 0.2416 | 4.548647 | 5.40E-06 | 2.14E-04 | UP   |
| BMP1      | 3842.361143 | 1.089052 | 0.2108 | 5.166287 | 2.39E-07 | 1.96E-05 | UP   |
| TAPBP     | 8126.944828 | 1.083942 | 0.2448 | 4.428007 | 9.51E-06 | 3.33E-04 | UP   |
| GRN       | 16966.38163 | 1.069879 | 0.2165 | 4.941802 | 7.74E-07 | 4.95E-05 | UP   |
| TRIM16L   | 1702.597025 | 1.063636 | 0.2242 | 4.743571 | 2.10E-06 | 1.08E-04 | UP   |
| FZD2      | 585.256609  | 1.060629 | 0.1901 | 5.579727 | 2.41E-08 | 3.03E-06 | UP   |
| CERCAM    | 1327.347272 | 1.05838  | 0.2222 | 4.762538 | 1.91E-06 | 1.01E-04 | UP   |
| HDAC5     | 1286.975423 | 1.056181 | 0.2139 | 4.937904 | 7.90E-07 | 5.01E-05 | UP   |
| SOCS2     | 743.9814851 | 1.054983 | 0.2290 | 4.606529 | 4.09E-06 | 1.75E-04 | UP   |
| LZTS3     | 1131.107058 | 1.050957 | 0.1791 | 5.866479 | 4.45E-09 | 8.65E-07 | UP   |
| LAMA5     | 14438.16719 | 1.047552 | 0.1876 | 5.585432 | 2.33E-08 | 3.01E-06 | UP   |
| HLA-A     | 19277.68154 | 1.043102 | 0.2010 | 5.18877  | 2.12E-07 | 1.77E-05 | UP   |
| NFIX      | 1155.02995  | 1.042092 | 0.2289 | 4.553181 | 5.28E-06 | 2.13E-04 | UP   |
| RHOB      | 1629.603892 | 1.041269 | 0.2322 | 4.483952 | 7.33E-06 | 2.75E-04 | UP   |
| PLPP1     | 969.6634603 | 1.038481 | 0.2347 | 4.424384 | 9.67E-06 | 3.37E-04 | UP   |
| KREMEN1   | 401.235563  | 1.035767 | 0.1902 | 5.445745 | 5.16E-08 | 5.62E-06 | UP   |
| DISP2     | 320.1215539 | 1.035276 | 0.1727 | 5.994119 | 2.05E-09 | 4.64E-07 | UP   |
| AJUBA     | 7921.532093 | 1.02498  | 0.1860 | 5.510061 | 3.59E-08 | 4.22E-06 | UP   |
| SMPD1     | 1039.565033 | 1.02478  | 0.2096 | 4.889002 | 1.01E-06 | 6.18E-05 | UP   |
| PTPRR     | 507.3985128 | 1.023338 | 0.2254 | 4.540014 | 5.63E-06 | 2.21E-04 | UP   |
| FADS3     | 968.6341321 | 1.012943 | 0.2270 | 4.463168 | 8.08E-06 | 2.94E-04 | UP   |
| TAP1      | 3029.46795  | 1.005927 | 0.2209 | 4.553196 | 5.28E-06 | 2.13E-04 | UP   |
| MMP14     | 10630.14201 | 1.00274  | 0.2035 | 4.927348 | 8.34E-07 | 5.20E-05 | UP   |
| NUP62CL   | 316.5617526 | -1.00056 | 0.2847 | -3.51448 | 4.41E-04 | 0.005354 | DOWN |
| PNP       | 1198.907053 | -1.0033  | 0.2498 | -4.01584 | 5.92E-05 | 0.001245 | DOWN |
| IRS1      | 1989.294014 | -1.01181 | 0.2192 | -4.61501 | 3.93E-06 | 1.70E-04 | DOWN |
| NGEF      | 434.5577662 | -1.01424 | 0.2754 | -3.68338 | 2.30E-04 | 0.003362 | DOWN |
| ASPH      | 30481.00088 | -1.0159  | 0.2232 | -4.5516  | 5.32E-06 | 2.14E-04 | DOWN |
| WDHD1     | 1389.210761 | -1.01945 | 0.2676 | -3.81003 | 1.39E-04 | 0.002339 | DOWN |
| ERRFI1    | 4565.837496 | -1.02084 | 0.2420 | -4.21887 | 2.46E-05 | 6.67E-04 | DOWN |
| KNSTRN    | 1841.076588 | -1.02292 | 0.2955 | -3.46207 | 5.36E-04 | 0.006125 | DOWN |
| TNFRSF10A | 484.2506724 | -1.02995 | 0.1907 | -5.40199 | 6.59E-08 | 6.76E-06 | DOWN |
| SSFA2     | 12258.70933 | -1.03508 | 0.1807 | -5.72951 | 1.01E-08 | 1.59E-06 | DOWN |
| PSMC3IP   | 267.3076108 | -1.03735 | 0.2426 | -4.27613 | 1.90E-05 | 5.58E-04 | DOWN |
| RFC3      | 1754.632341 | -1.03779 | 0.2905 | -3.57225 | 3.54E-04 | 0.00454  | DOWN |
| F2RL1     | 3786.841719 | -1.04306 | 0.2038 | -5.11702 | 3.10E-07 | 2.43E-05 | DOWN |
| MERTK     | 480.2462341 | -1.04955 | 0.2280 | -4.60317 | 4.16E-06 | 1.76E-04 | DOWN |
| SPRED3    | 92.48201694 | -1.05145 | 0.2567 | -4.09533 | 4.22E-05 | 9.91E-04 | DOWN |
| DNMBP     | 2787.869514 | -1.06265 | 0.2535 | -4.19148 | 2.77E-05 | 7.37E-04 | DOWN |
| STN1      | 1587.859349 | -1.06388 | 0.1584 | -6.7184  | 1.84E-11 | 8.33E-09 | DOWN |
| GMNN      | 1249.498695 | -1.06518 | 0.2352 | -4.5279  | 5.96E-06 | 2.31E-04 | DOWN |
| TBC1D8    | 1920.493006 | -1.0711  | 0.2200 | -4.86948 | 1.12E-06 | 6.70E-05 | DOWN |
| CDKN3     | 1530.075342 | -1.07913 | 0.3148 | -3.4281  | 6.08E-04 | 0.00675  | DOWN |
| RFC4      | 1464.081512 | -1.08774 | 0.2443 | -4.45247 | 8.49E-06 | 3.03E-04 | DOWN |
| FAM3C     | 7721.256556 | -1.09035 | 0.2631 | -4.14452 | 3.41E-05 | 8.54E-04 | DOWN |
| LIF       | 1889.190478 | -1.09481 | 0.2889 | -3.79006 | 1.51E-04 | 0.002451 | DOWN |
| VRK1      | 1150.263711 | -1.0988  | 0.2639 | -4.16323 | 3.14E-05 | 8.04E-04 | DOWN |
| TEX30     | 673.5454314 | -1.11117 | 0.2239 | -4.96217 | 6.97E-07 | 4.54E-05 | DOWN |
| CTSC      | 7283.398267 | -1.11217 | 0.1886 | -5.89731 | 3.69E-09 | 7.47E-07 | DOWN |
| LHX1      | 190.5782665 | -1.13616 | 0.2598 | -4.37339 | 1.22E-05 | 4.00E-04 | DOWN |
| STMN3     | 636.5538366 | -1.14608 | 0.2766 | -4.14388 | 3.41E-05 | 8.54E-04 | DOWN |
| MPV17L    | 152.3831798 | -1.15389 | 0.2203 | -5.23734 | 1.63E-07 | 1.43E-05 | DOWN |
| SPRY1     | 627.0916325 | -1.15856 | 0.2835 | -4.08702 | 4.37E-05 | 0.00101  | DOWN |

|           |             |          |        |          |          |          |      |
|-----------|-------------|----------|--------|----------|----------|----------|------|
| HMGB2     | 5873.237271 | -1.16257 | 0.2733 | -4.25331 | 2.11E-05 | 5.96E-04 | DOWN |
| CENPW     | 598.2560388 | -1.16723 | 0.3255 | -3.58586 | 3.36E-04 | 0.004415 | DOWN |
| CENPK     | 1201.343114 | -1.16778 | 0.3062 | -3.81347 | 1.37E-04 | 0.002318 | DOWN |
| LYAR      | 914.4195624 | -1.17261 | 0.2537 | -4.62198 | 3.80E-06 | 1.65E-04 | DOWN |
| CHAC2     | 269.5839137 | -1.1895  | 0.2356 | -5.04945 | 4.43E-07 | 3.19E-05 | DOWN |
| CDC6      | 2050.719239 | -1.19256 | 0.3267 | -3.65032 | 2.62E-04 | 0.003688 | DOWN |
| SPRY2     | 944.4278081 | -1.19405 | 0.2755 | -4.33462 | 1.46E-05 | 4.55E-04 | DOWN |
| ZWINT     | 3297.695911 | -1.19774 | 0.3429 | -3.49334 | 4.77E-04 | 0.005664 | DOWN |
| CDHR3     | 149.4337754 | -1.19943 | 0.1766 | -6.79073 | 1.12E-11 | 5.36E-09 | DOWN |
| STK32B    | 332.1113955 | -1.19945 | 0.2933 | -4.08911 | 4.33E-05 | 0.001008 | DOWN |
| FAM81A    | 130.5539011 | -1.2025  | 0.2786 | -4.3168  | 1.58E-05 | 4.83E-04 | DOWN |
| POLR3G    | 504.6038484 | -1.20985 | 0.2850 | -4.24578 | 2.18E-05 | 6.12E-04 | DOWN |
| LSAMP     | 102.1530078 | -1.22536 | 0.3414 | -3.5897  | 3.31E-04 | 0.004374 | DOWN |
| PTTG1     | 2964.138376 | -1.23234 | 0.3609 | -3.41479 | 6.38E-04 | 0.007046 | DOWN |
| EMP1      | 8467.430621 | -1.24649 | 0.2820 | -4.41947 | 9.89E-06 | 3.42E-04 | DOWN |
| SPRED1    | 1177.072592 | -1.24721 | 0.2209 | -5.64522 | 1.65E-08 | 2.37E-06 | DOWN |
| PLK3      | 448.5384545 | -1.24869 | 0.3173 | -3.93522 | 8.31E-05 | 0.001589 | DOWN |
| RHEBL1    | 69.11557677 | -1.2541  | 0.2986 | -4.20052 | 2.66E-05 | 7.14E-04 | DOWN |
| UBE2T     | 1744.073367 | -1.25543 | 0.2999 | -4.18648 | 2.83E-05 | 7.49E-04 | DOWN |
| FAM216A   | 362.9145908 | -1.25584 | 0.2961 | -4.24072 | 2.23E-05 | 6.22E-04 | DOWN |
| ARG2      | 144.1617882 | -1.25595 | 0.2642 | -4.75321 | 2.00E-06 | 1.05E-04 | DOWN |
| MMD       | 1110.029403 | -1.2561  | 0.3028 | -4.14783 | 3.36E-05 | 8.52E-04 | DOWN |
| PRIM1     | 523.2764018 | -1.26387 | 0.3403 | -3.71409 | 2.04E-04 | 0.003062 | DOWN |
| KIAA1755  | 65.86997806 | -1.27607 | 0.3250 | -3.92681 | 8.61E-05 | 0.001631 | DOWN |
| NUF2      | 1530.082739 | -1.27799 | 0.3696 | -3.45774 | 5.45E-04 | 0.006215 | DOWN |
| RIBC2     | 193.4405016 | -1.28251 | 0.2732 | -4.69486 | 2.67E-06 | 1.27E-04 | DOWN |
| XDH       | 228.038736  | -1.28426 | 0.3722 | -3.45012 | 5.60E-04 | 0.006364 | DOWN |
| CDCA7     | 1005.598677 | -1.288   | 0.3047 | -4.22713 | 2.37E-05 | 6.50E-04 | DOWN |
| PITPNC1   | 368.6599464 | -1.292   | 0.2933 | -4.40459 | 1.06E-05 | 3.55E-04 | DOWN |
| MILR1     | 377.2920219 | -1.29633 | 0.3553 | -3.64853 | 2.64E-04 | 0.003707 | DOWN |
| OTUB2     | 326.7279526 | -1.29922 | 0.3101 | -4.1902  | 2.79E-05 | 7.40E-04 | DOWN |
| MAD2L1    | 2197.494978 | -1.29942 | 0.3095 | -4.19903 | 2.68E-05 | 7.17E-04 | DOWN |
| PBK       | 1630.748248 | -1.3332  | 0.3724 | -3.57958 | 3.44E-04 | 0.004472 | DOWN |
| MAFF      | 800.0323248 | -1.33548 | 0.2779 | -4.80494 | 1.55E-06 | 8.71E-05 | DOWN |
| SOX7      | 784.37094   | -1.34904 | 0.2839 | -4.75126 | 2.02E-06 | 1.06E-04 | DOWN |
| CORO1A    | 123.4502227 | -1.34942 | 0.3285 | -4.10766 | 4.00E-05 | 9.56E-04 | DOWN |
| PGF       | 77.27639839 | -1.39948 | 0.3622 | -3.86332 | 1.12E-04 | 0.001979 | DOWN |
| PRDM8     | 329.4368657 | -1.45175 | 0.2585 | -5.6153  | 1.96E-08 | 2.65E-06 | DOWN |
| C6orf141  | 426.5466887 | -1.46955 | 0.3199 | -4.59416 | 4.34E-06 | 1.82E-04 | DOWN |
| DNAH2     | 187.5592472 | -1.47593 | 0.3322 | -4.44257 | 8.89E-06 | 3.15E-04 | DOWN |
| GJB2      | 729.7424999 | -1.48296 | 0.3830 | -3.87233 | 1.08E-04 | 0.00193  | DOWN |
| ST3GAL6   | 228.3759087 | -1.50178 | 0.3205 | -4.68642 | 2.78E-06 | 1.32E-04 | DOWN |
| UBASH3B   | 1555.902875 | -1.50889 | 0.2584 | -5.84012 | 5.22E-09 | 9.76E-07 | DOWN |
| LYZ       | 14817.23629 | -1.51569 | 0.2548 | -5.94743 | 2.72E-09 | 6.00E-07 | DOWN |
| TNFSF15   | 1957.364353 | -1.51851 | 0.4132 | -3.67485 | 2.38E-04 | 0.003455 | DOWN |
| KIAA0040  | 1829.482929 | -1.52243 | 0.2934 | -5.18814 | 2.12E-07 | 1.77E-05 | DOWN |
| KIAA1549L | 422.4071464 | -1.52394 | 0.4015 | -3.79543 | 1.47E-04 | 0.002418 | DOWN |
| IGFBP1    | 74.59407813 | -1.52938 | 0.3690 | -4.14447 | 3.41E-05 | 8.54E-04 | DOWN |
| HAS3      | 810.1496077 | -1.53763 | 0.3275 | -4.69496 | 2.67E-06 | 1.27E-04 | DOWN |
| SLC45A3   | 662.766023  | -1.5681  | 0.4289 | -3.65617 | 2.56E-04 | 0.003626 | DOWN |
| AGR2      | 5991.112444 | -1.56876 | 0.4539 | -3.45608 | 5.48E-04 | 0.006244 | DOWN |
| LRP8      | 1725.242386 | -1.57009 | 0.2642 | -5.94358 | 2.79E-09 | 6.05E-07 | DOWN |
| GPAT3     | 928.7554457 | -1.58502 | 0.3016 | -5.25578 | 1.47E-07 | 1.31E-05 | DOWN |
| GALNT14   | 303.6830518 | -1.61042 | 0.3899 | -4.12987 | 3.63E-05 | 8.94E-04 | DOWN |
| TM4SF18   | 1864.432575 | -1.61271 | 0.3892 | -4.14363 | 3.42E-05 | 8.54E-04 | DOWN |
| SPRED2    | 1229.033561 | -1.61947 | 0.2740 | -5.90966 | 3.43E-09 | 7.32E-07 | DOWN |
| ITPRIPL1  | 94.16712057 | -1.62825 | 0.4028 | -4.04183 | 5.30E-05 | 0.001147 | DOWN |
| TLR4      | 788.0897591 | -1.64573 | 0.2859 | -5.75636 | 8.59E-09 | 1.45E-06 | DOWN |
| TRIB2     | 1467.270082 | -1.66434 | 0.4223 | -3.94104 | 8.11E-05 | 0.001559 | DOWN |
| LAT2      | 157.8773572 | -1.67192 | 0.3549 | -4.7103  | 2.47E-06 | 1.23E-04 | DOWN |
| EREG      | 2775.444546 | -1.70807 | 0.3863 | -4.42121 | 9.82E-06 | 3.40E-04 | DOWN |

|          |             |          |        |          |          |          |      |
|----------|-------------|----------|--------|----------|----------|----------|------|
| STAMBPL1 | 564.7156505 | -1.73474 | 0.2342 | -7.40747 | 1.29E-13 | 9.64E-11 | DOWN |
| CNIH3    | 296.7965264 | -1.74809 | 0.3014 | -5.80056 | 6.61E-09 | 1.18E-06 | DOWN |
| FOXL1    | 836.0781376 | -1.75188 | 0.3442 | -5.09039 | 3.57E-07 | 2.71E-05 | DOWN |
| KRT23    | 787.2115334 | -1.75991 | 0.4657 | -3.77935 | 1.57E-04 | 0.002505 | DOWN |
| ITGA2    | 7529.33203  | -1.81745 | 0.3619 | -5.02213 | 5.11E-07 | 3.56E-05 | DOWN |
| DUSP4    | 3954.154388 | -1.83919 | 0.2990 | -6.15178 | 7.66E-10 | 2.01E-07 | DOWN |
| AK5      | 108.5031296 | -1.8559  | 0.3852 | -4.81859 | 1.45E-06 | 8.26E-05 | DOWN |
| CLDN2    | 151.2394452 | -1.86504 | 0.4752 | -3.92434 | 8.70E-05 | 0.001644 | DOWN |
| ANXA10   | 1149.622804 | -1.894   | 0.4999 | -3.78901 | 1.51E-04 | 0.002453 | DOWN |
| HAS2     | 225.4103511 | -1.90076 | 0.4007 | -4.74332 | 2.10E-06 | 1.08E-04 | DOWN |
| CALB2    | 121.820401  | -1.91554 | 0.4294 | -4.46054 | 8.18E-06 | 2.95E-04 | DOWN |
| RGS2     | 788.2388653 | -1.91554 | 0.2795 | -6.85382 | 7.19E-12 | 3.84E-09 | DOWN |
| CXCR4    | 214.3020476 | -1.92503 | 0.3773 | -5.10194 | 3.36E-07 | 2.58E-05 | DOWN |
| ONCUT3   | 472.6530867 | -1.95094 | 0.5343 | -3.65157 | 2.61E-04 | 0.003677 | DOWN |
| HS3ST1   | 895.6719463 | -1.96367 | 0.3924 | -5.00456 | 5.60E-07 | 3.83E-05 | DOWN |
| SBK3     | 23.25275833 | -1.97144 | 0.5121 | -3.84963 | 1.18E-04 | 0.002061 | DOWN |
| RXFP4    | 27.35742117 | -1.98706 | 0.4826 | -4.11752 | 3.83E-05 | 9.26E-04 | DOWN |
| ANKRD22  | 177.4804556 | -2.02294 | 0.4456 | -4.54022 | 5.62E-06 | 2.21E-04 | DOWN |
| IL1RAPL1 | 47.09528635 | -2.05323 | 0.6013 | -3.41438 | 6.39E-04 | 0.007052 | DOWN |
| HMGA2    | 1837.556522 | -2.06593 | 0.3412 | -6.05514 | 1.40E-09 | 3.28E-07 | DOWN |
| CST2     | 197.4361702 | -2.13792 | 0.4488 | -4.76385 | 1.90E-06 | 1.01E-04 | DOWN |
| PTX3     | 199.1429575 | -2.20927 | 0.4777 | -4.62451 | 3.75E-06 | 1.63E-04 | DOWN |
| PHLDA1   | 4506.493934 | -2.23113 | 0.2533 | -8.80737 | 1.28E-18 | 3.35E-15 | DOWN |
| NT5E     | 5982.121094 | -2.27449 | 0.3416 | -6.65785 | 2.78E-11 | 1.12E-08 | DOWN |
| HMGA1    | 8942.602366 | -2.28914 | 0.3956 | -5.78602 | 7.21E-09 | 1.25E-06 | DOWN |
| GPR3     | 31.40140251 | -2.29063 | 0.6646 | -3.44661 | 5.68E-04 | 0.006415 | DOWN |
| GMFG     | 45.30947569 | -2.29751 | 0.5259 | -4.36864 | 1.25E-05 | 4.07E-04 | DOWN |
| TNS4     | 2949.129438 | -2.31434 | 0.3367 | -6.87342 | 6.27E-12 | 3.47E-09 | DOWN |
| SRPX2    | 683.7213328 | -2.31467 | 0.4086 | -5.6651  | 1.47E-08 | 2.22E-06 | DOWN |
| MT1A     | 40.92816294 | -2.32062 | 0.4559 | -5.08975 | 3.59E-07 | 2.71E-05 | DOWN |
| TCN1     | 314.3879522 | -2.32367 | 0.4002 | -5.80663 | 6.37E-09 | 1.15E-06 | DOWN |
| SLCO4A1  | 2532.302908 | -2.34576 | 0.4863 | -4.82358 | 1.41E-06 | 8.12E-05 | DOWN |
| TOX2     | 219.2226417 | -2.42222 | 0.3569 | -6.78691 | 1.15E-11 | 5.36E-09 | DOWN |
| TFF1     | 77.45782221 | -2.49932 | 0.6100 | -4.09703 | 4.18E-05 | 9.88E-04 | DOWN |
| AREG     | 1121.035064 | -2.5124  | 0.4596 | -5.46684 | 4.58E-08 | 5.23E-06 | DOWN |
| MUC5AC   | 1237.087334 | -2.5162  | 0.6463 | -3.89332 | 9.89E-05 | 0.001805 | DOWN |
| RGS4     | 775.2144114 | -2.70122 | 0.3662 | -7.37691 | 1.62E-13 | 1.15E-10 | DOWN |
| FOSL1    | 2439.159881 | -2.71197 | 0.4662 | -5.81675 | 6.00E-09 | 1.10E-06 | DOWN |
| NTSR1    | 1521.213248 | -2.78522 | 0.4436 | -6.27899 | 3.41E-10 | 1.02E-07 | DOWN |
| EGR1     | 241.158573  | -2.81263 | 0.7053 | -3.98794 | 6.66E-05 | 0.001354 | DOWN |
| EV12B    | 72.34161187 | -2.84146 | 0.4728 | -6.0093  | 1.86E-09 | 4.29E-07 | DOWN |
| CST1     | 157.833506  | -2.8421  | 0.4297 | -6.61463 | 3.72E-11 | 1.43E-08 | DOWN |
| LGALS9B  | 28.91281009 | -2.95145 | 0.7668 | -3.84899 | 1.19E-04 | 0.002064 | DOWN |
| COL13A1  | 300.4556311 | -3.01033 | 0.4319 | -6.96939 | 3.18E-12 | 1.83E-09 | DOWN |
| CAPN8    | 949.2501046 | -3.05093 | 0.4060 | -7.51487 | 5.70E-14 | 4.74E-11 | DOWN |
| PIWIL1   | 17.30978303 | -3.19213 | 0.5794 | -5.50895 | 3.61E-08 | 4.22E-06 | DOWN |
| SH2D1B   | 20.13449612 | -3.20521 | 0.6683 | -4.7961  | 1.62E-06 | 8.94E-05 | DOWN |
| MYH15    | 283.6084394 | -3.23042 | 0.5149 | -6.27377 | 3.52E-10 | 1.03E-07 | DOWN |
| MYEOV    | 2202.079766 | -3.23269 | 0.4310 | -7.50117 | 6.33E-14 | 4.98E-11 | DOWN |
| DMBT1    | 791.2874003 | -3.29839 | 0.8694 | -3.79369 | 1.48E-04 | 0.002431 | DOWN |
| CST4     | 187.9512295 | -3.30601 | 0.5124 | -6.45234 | 1.10E-10 | 3.75E-08 | DOWN |
| IL1RL1   | 56.01295161 | -3.3736  | 0.6043 | -5.58239 | 2.37E-08 | 3.01E-06 | DOWN |
| LGALS9C  | 136.2398653 | -3.57789 | 1.0395 | -3.44201 | 5.77E-04 | 0.006482 | DOWN |
| ETV1     | 440.1125354 | -3.82411 | 0.4053 | -9.43429 | 3.94E-21 | 1.96E-17 | DOWN |
| ASB2     | 13.95156205 | -3.84037 | 0.7045 | -5.45101 | 5.01E-08 | 5.60E-06 | DOWN |
| ETV4     | 803.5006065 | -3.96787 | 0.4988 | -7.95508 | 1.79E-15 | 2.23E-12 | DOWN |
| SPRY4    | 659.1047847 | -4.11659 | 0.4793 | -8.588   | 8.85E-18 | 1.66E-14 | DOWN |
| ETV5     | 580.3549573 | -4.15173 | 0.4170 | -9.95707 | 2.35E-23 | 3.52E-19 | DOWN |
| DUSP6    | 2474.533565 | -4.52296 | 0.4614 | -9.8024  | 1.10E-22 | 8.23E-19 | DOWN |

